THE JOURNAL OF BIOLOGICAL CHEMISTRY VOL. 288, NO. 21, pp. 15212–15228, May 24, 2013

Regulatory Interactions between a Bacterial Tyrosine Kinase and Its Cognate Phosphatase*

Received for publication, January 29, 2013, and in revised form, March 28, 2013 Published, JBC Papers in Press, March 30, 2013, DOI 10.1074/jbc.M113.457804

Deniz B. Temel[‡§1], Kaushik Dutta[¶1,2], Sébastien Alphonse[‡], Julien Nourikyan[‖], Christophe Grangeasse[‖], and Ranajeet Ghose[‡§3]

From the [‡]Department of Chemistry, City College of New York, New York, New York 10031, the [§]Graduate Center of the City University of New York, New York, New York 10016, the [¶]New York Structural Biology Center, New York, New York 10027, and the [‖]Institut de Biologie et Chimie des Protéines, BMSSI-UMR 5086, CNRS, Université Lyon 1, Université de Lyon, 69367 Lyon, France

Background: Wzb phosphatase dephosphorylates Wzc tyrosine kinase in *E. coli*.
Results: We have characterized the regulatory interactions between Wzb and Wzc.
Conclusion: Wzb-catalyzed Wzc dephosphorylation relies on the increased local concentration of substrate due to mutual docking interactions.
Significance: Structural elements that mediate the interactions between a bacterial tyrosine kinase and its cognate phosphatase have been ascertained for the very first time.

The cyclic process of autophosphorylation of the C-terminal tyrosine cluster (YC) of a bacterial tyrosine kinase and its subsequent dephosphorylation following interactions with a counteracting tyrosine phosphatase regulates diverse physiological processes, including the biosynthesis and export of polysaccharides responsible for the formation of biofilms or virulence-determining capsules. We provide here the first detailed insight into this hitherto uncharacterized regulatory interaction at residue-specific resolution using *Escherichia coli* Wzc, a canonical bacterial tyrosine kinase, and its opposing tyrosine phosphatase, Wzb. The phosphatase Wzb utilizes a surface distal to the catalytic elements of the kinase, Wzc, to dock onto its catalytic domain (Wzc_{CD}). Wzc_{CD} binds in a largely YC-independent fashion near the Wzb catalytic site, inducing allosteric changes therein. YC dephosphorylation is proximity-mediated and reliant on the elevated concentration of phosphorylated YC near the Wzb active site resulting from Wzc_{CD} docking. Wzb principally recognizes the phosphate of its phosphotyrosine substrate and further stabilizes the tyrosine moiety through ring stacking interactions with a conserved active site tyrosine.

Tyrosine phosphorylation has been long realized to be a critical signaling mechanism in higher eukaryotes (1) that is responsible for almost every aspect of cell growth, differentiation, maturation, motility, and regulated cell death. On the other hand, although the existence of tyrosine phosphorylation in bacteria has been known for quite some time (2–4), its influence on bacterial physiology has been largely ignored. However, with mounting evidence of the role of tyrosine kinase signaling in the virulence of many pathogenic bacteria (5–7), its critical role in bacterial cell signaling is gaining prominence (8–11).

The bacterial tyrosine kinase (BY-kinase)[4] family (10–12) that is highly conserved (13) in both Gram-negative and Gram-positive species constitutes the largest family of protein-tyrosine kinases (PTKs) in bacteria. The central role of BY-kinase-mediated signal transduction in the synthesis and export of polysaccharides responsible for biofilm or capsule formation (9, 10, 12) is well established. In addition, BY-kinases also appear to participate in diverse cellular processes, including antibiotic resistance (14), lysogenization (15), and DNA metabolism (16), indicating that the extent of their influence on bacterial physiology could rival that seen for PTKs in life's critical processes in higher eukaryotes (17).

BY-kinases comprise a periplasmic/extracytoplasmic domain, two trans-membrane helices, and a cytoplasmic catalytic domain (CD) that is structurally distinct from those found in eukaryotic PTKs. Recently solved structures of the CDs of several BY-kinases, including Etk (18) and Wzc (19) (Fig. 1) from *Escherichia coli* and CapB from *Staphylococcus aureus* (20), confirmed their unique features highlighted by an absence of the two-lobed fold characteristic of the CDs of eukaryotic PTKs. Also striking was the close structural similarity of the BY-kinases to P-loop ATPases. BY-kinase CDs possess ATP-binding motifs reminiscent of the Walker motifs of P-loop ATPases instead of eukaryal kinase sequence motifs (21). These motifs include the following (Fig. 1): Walker A ((A/G)*XXXXX*GK(S/T); usually only the GK(S/T) element is conserved in BY-kinases); Walker B ($\phi\phi\phi\phi$D*XX*P, where ϕ is a hydro-

* This work was supported, in whole or in part, by National Institutes of Health Grants GM084278 and AI101792. This work was also supported by CNRS, Université de Lyon, and the Agence National de la Recherche (ANR-08-BLAN-0143 and ANR-10-BLAN-1303-01). The NMR facilities at City College of New York are partially supported by National Institutes of Health Grants 2G12RR03060 and 8G12MD007603. Facilities at the New York Structural Biology Center are supported by National Institutes of Health Grants CO6RR015495 and P41GM066354; the New York State Office for Science, Technology, and Academic Research (NYSTAR); the Keck Foundation; and the New York City Economic Development Corporation.
[1] Both authors contributed equally to this work.
[2] To whom correspondence may be addressed: New York Structural Biology Center, 89 Convent Ave., New York, NY 10027. Tel.: 212-939-0660 (ext. 9304); Fax: 212-939-0863; E-mail: dutta@nysbc.org.
[3] To whom correspondence may be addressed: Dept. of Chemistry, City College of New York, 160 Convent Ave., New York, NY 10031. Tel.: 212-650-6049; Fax: 212-650-6107; E-mail: rghose@sci.ccny.cuny.edu.

[4] The abbreviations used are: BY-kinase, bacterial tyrosine kinase; PTK, protein-tyrosine kinase; PTP, protein tyrosine phosphatase; LMW-PTP, low molecular weight PTP; CD, catalytic domain; TROSY, transverse relaxation optimized spectroscopy; BisTris, 2-[bis(2-hydroxyethyl)amino]-2-(hydroxymethyl)propane-1,3-diol; SPR, surface plasmon resonance; YC, tyrosine cluster.

phobic residue; the *XX*P sequence is a BY-kinase-specific extension of the Walker B motif); and an additional motif that is similar to a Walker B, called the Walker A′ ($\phi\phi\phi\phi$D*X*D*X*R) (11, 22).

Regulation of BY-kinases occurs through the intermolecular autophosphorylation and subsequent dephosphorylation of 3–7 tyrosine residues (the tyrosine cluster (YC)) located on the C-terminal tail (C-tail) (Fig. 1*B*) of the CD. Based on extensive biochemical and *in vivo* evidence (23), it is apparent that BY-kinases cannot be classified as being in "active" or "inactive" states, as for a majority of eukaryotic kinases, dependent simply on the phosphorylation state of key regulatory residues (24–27). It is also clear that the overall level of YC phosphorylation rather than the quantitative phosphorylation state of any specific YC tyrosine is important for activity (28, 29). Thus, the current model for BY-kinase activity suggests that activity is related to the cycling between a state where the YC is highly phosphorylated (YC_{high}) and a state where the level of YC phosphorylation is greatly reduced (YC_{low}); the presence of both of these states is essential in cellular physiology (10).

Generation of the YC_{high} state is achieved by intermolecular autophosphorylation facilitated by the oligomerization of the cytoplasmic CDs of the BY-kinases in which the YC of one subunit (substrate-acting) is inserted into the catalytic site of the neighboring subunit (enzyme-acting) in the oligomer, as in the case of eukaryotic PTKs (30). A highly conserved sequence motif (E*XX*R*XX*R) has been shown to be critical in facilitating the self-association of the CDs of the BY-kinases necessary to accomplish trans-phosphorylation. There are three specific lines of evidence for this. (i) This motif has been shown to play a central role in generating the octameric oligomerization state seen in the crystal structures of the CDs of Wzc (19) as well as *S. aureus* CapB (20), hinting at a general mode of oligomerization and trans-phosphorylation. (ii) Although the isolated CDs of BY-kinases are largely monomeric in solution (as will be demonstrated below), analytical gel filtration revealed the presence of a minor population of a high molecular weight species for the CD of a Wzc mutant (K540M) that cannot bind ATP and hence is incapable of generating a YC_{high} state. This high molecular weight species was eliminated by mutating the conserved residues of the E*XX*R*XX*R motif to alanine (19). (iii) This same triple mutation reduced the autophosphorylation levels of Wzc (in the context of full-length protein) to around 10% of wild type (19), suggesting its importance for trans-phosphorylation. Although the tendency of the isolated BY-kinase CDs to oligomerize in solution appears to be low, this low self-affinity is likely to be enhanced severalfold in the context of the membrane-bound fully assembled signaling complex that involves additional interactions involving the periplasmic domains and perhaps the membrane segments (31). However, it is to be noted that isolated BY-kinase CDs have been shown to form higher order oligomers *in vivo* (29) using formaldehyde cross-linking. Thus, based on the current state of knowledge, the following hypothesis for BY-kinase regulation may be proposed. An association of the CDs is followed by trans-phosphorylation and generation of a YC_{high} state. The CDs in the YC_{high} state then dissociate to expose the active site (occluded in the oligomeric state) to downstream targets, such as UDP glucose dehydrogenase, a known BY-kinase target in both Gram-negative (32) and Gram-positive species (33). Regeneration of the YC_{low} state of the CD occurs by the action of protein-tyrosine phosphatases (PTPs), and this reinitiates the cycle. Therefore, this cycling between YC_{high} and YC_{low} states and consequently between associated and dissociated states of the CD appears key for maintaining function (10). Thus, the critical players in sustaining this YC_{high}/YC_{low} cycle that occurs in the cytoplasm are the bacterial PTPs. Several of these PTPs belong to the low molecular weight protein-tyrosine phosphatase (LMW-PTP, also known as class II PTP) family.

Bacterial LMW-PTPs are wholly cytosolic and eukaryotic-like in overall structure (34–37) (Fig. 2), although they lack several key features considered to be important for substrate recognition in eukaryotes, suggesting unique mechanisms of kinase docking and regulation. Functional BY-kinase/LMW-PTP pairs in bacteria include Wzc/Wzb (38) and Etk/Etp (*E. coli*) (39), Ptk/Ptp (*Acinetobacter johnsonii*) (40), and Yco6/Yor5 (*Klebsiella pneumoniae*) (41), to name a few that have been characterized. Despite extensive genetic and biochemical evidence for the critical role of BY-kinase/LMW-PTP interactions in bacterial tyrosine phosphorylation-mediated signaling, no information is available on the structural elements on BY-kinases that are important for their interactions with LMW-PTPs. Further, although structural work on bacterial PTPs, including the solution structure of *E. coli* Wzb (34), has allowed the generation of specific hypotheses on phosphotyrosine recognition by these enzymes, information on the specific nature of substrate recognition and dephosphorylation is lacking.

Toward our long term goal of characterizing BY-kinase/LMW-PTP interactions that are key in maintaining the critical cycling between YC_{high} and YC_{low} states in terms of structure, dynamics, and mechanism, we have chosen the canonical BY-kinase *E. coli* Wzc and its opposing LMW-PTP, Wzb, as a prototypical BY-kinase/LMW-PTP pair.

wzb and *wzc* belong to a gene cluster (*cps*) (42) that is responsible for the synthesis and export of the exopolysaccharide, colanic acid (23, 43), an essential component of biofilms and part of a physiological response to osmotic shock, damage to the cellular envelope, desiccation, and similar environmental stress conditions. For example, in the pathogenic enterohemorrhagic *E. coli* (O157:H7), the causative agent of acute hemorrhagic diarrhea, colanic acid protects the bacterial cells from the acidic conditions of gastrointestinal fluid (44). The proper levels and size distribution of colanic acid are therefore essential for resistance and survival under stress, a process that is hindered in cells lacking either YC-phosphorylated Wzc or Wzc dephosphorylated specifically by Wzb (43).

Here, using a variety of biophysical and biochemical methods, including solution NMR spectroscopy, we define for the first time, the structural elements on the catalytic domain of Wzc (Wzc_{CD}) and on Wzb responsible for their mutual interactions. Our results also provide insight into the mechanism by which Wzb recognizes its substrate, the phosphorylated YC of Wzc_{CD}.

EXPERIMENTAL PROCEDURES

Expression and Purification of Wzc_{CD} and Wzb Constructs Used for Biophysical Studies—wzc_{CD}, $wzc_{CD\Delta C}$, and *wzb* were cloned into pET15b vectors, transformed into *E. coli* BL21 DE3 cells, and purified as described in detail previously (45) for Wzc_{CD} (the various constructs utilized in this study are shown in Fig. 3). All proteins contained a thrombin-cleavable 21-resi-

due N-terminal tag. This tag appeared to ensure the long term stability of the proteins for the NMR experiments and was therefore not cleaved. After purification, the Wzc_{CD} and $Wzc_{CD\Delta C}$ samples were incubated overnight with a 25-fold excess of ATP/$MgCl_2$ followed by exchange against NMR buffer (see below) to remove the excess ATP. The *wzc*$_{CD,ERR/A}$

A

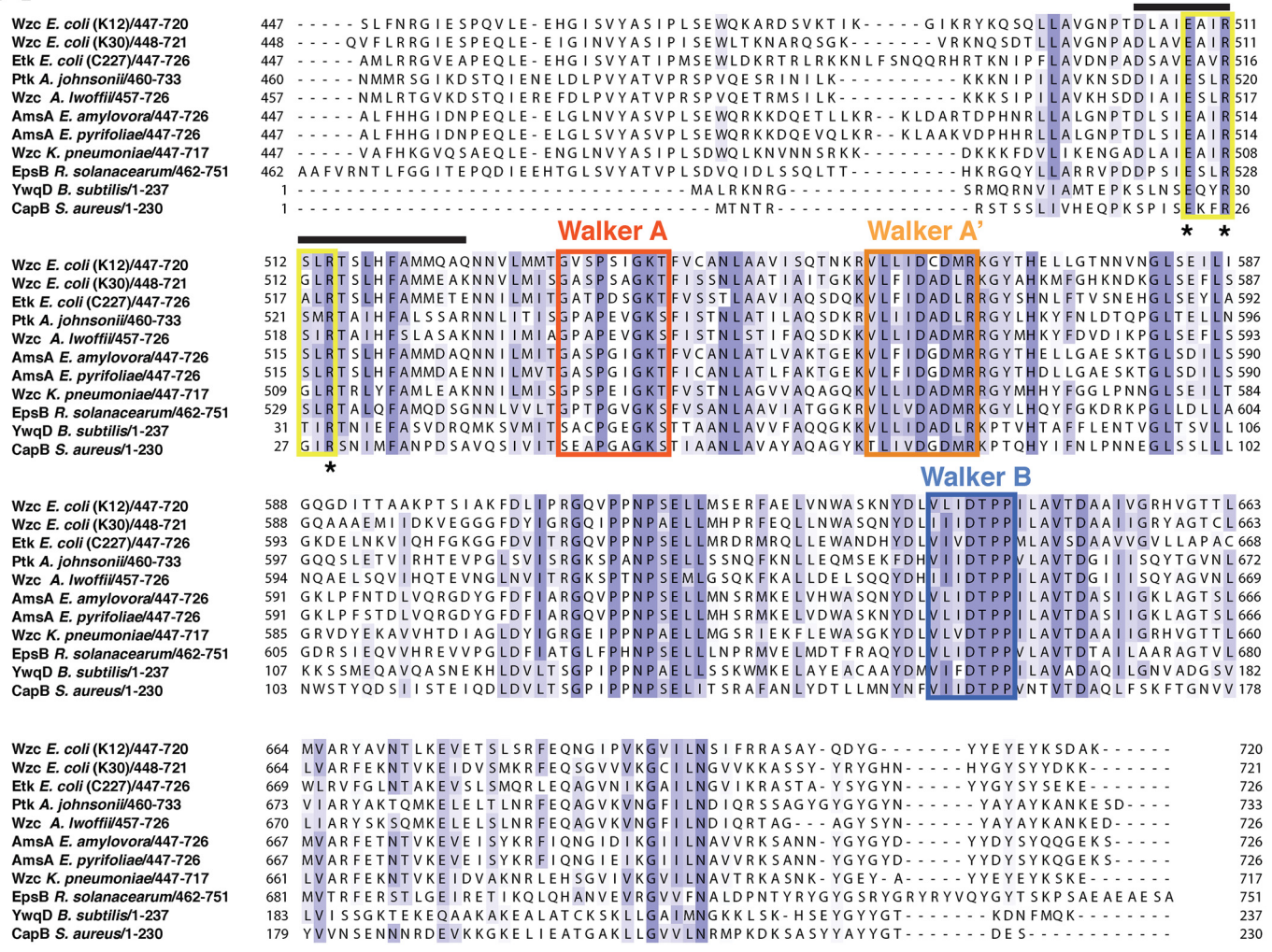

B

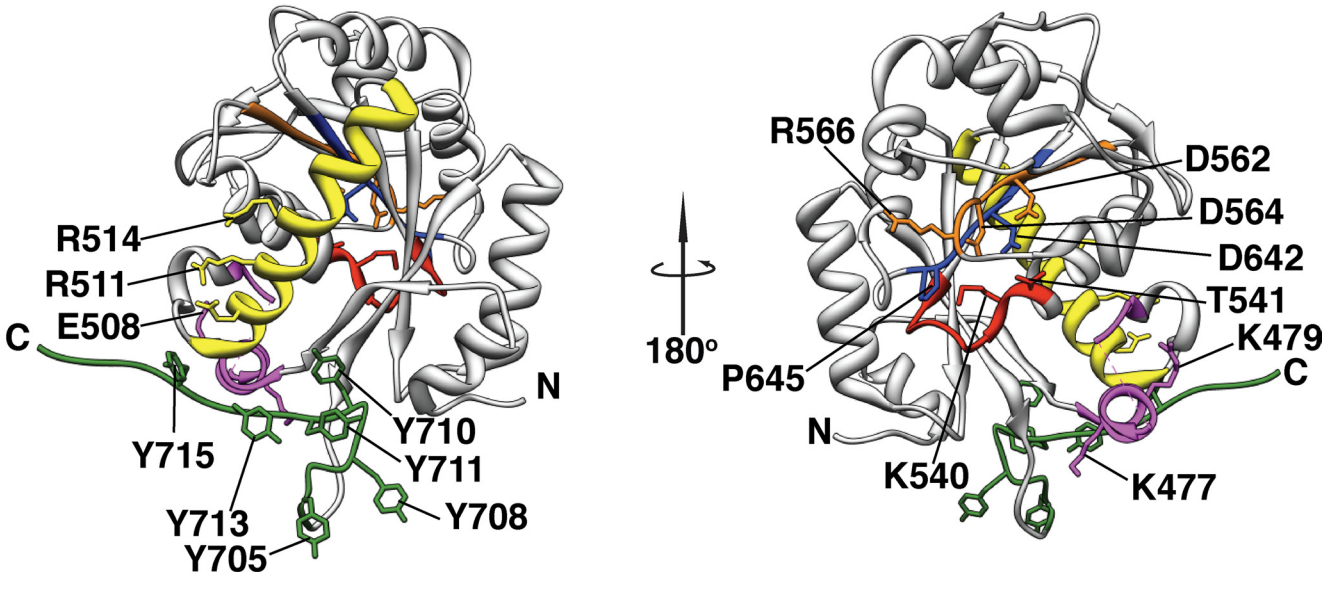

and wzb_{C9S} mutants were prepared from wzc_{CD} and *wzb*, respectively, using the QuikChange kit (Stratagene), cloned into pET15b, expressed, and purified as the corresponding wild-type proteins.

Expression and Purification of Wzc_{CD} Constructs Used for Enzymatic Assays—The DNA fragment encoding for wzc_{CD} was PCR-amplified using either the wild-type *E. coli* (K12) DNA or the pQE30-Wzc_{cyto}-ERR/A plasmid (19) and cloned into a pQE30 vector between the BamHI and HindIII restriction sites to generate wzc_{CD} (or the corresponding mutants: $wzc_{CD,ERR/A}$, $wzc_{CD,F5}$, and $wzc_{CD,F5,ERR/A}$). $Wzc_{CD,F5}$ and $Wzc_{CD,F5,ERR/A}$, both bearing N-terminal His_6 tags, were produced in *E. coli* Xl1-blue cells grown in LB medium supplemented with ampicillin and tetracycline. Overexpression was induced using 0.5 mM isopropyl 1-thio-β-D-galactopyranoside for 3 h at 37 °C when the A_{600} reached 0.4, followed by centrifugation for 10 min at 5000 × *g*. The pellet was re-suspended in 5 ml of buffer A (50 mM Tris-HCl, 200 mM NaCl, 10% glycerol, and 10 mM imidazole at pH 7.5) containing lysozyme (1 mg/liter), DNase I (6 mg/liter), and RNase A (6 mg/liter) by agitation for 15 min at 4 °C. Cells were lysed by sonication and centrifuged for 30 min at 14,000 × *g* at 4 °C. The supernatant was then mixed with nickel-nitrilotriacetic acid-agarose matrix (Qiagen) and incubated for 30 min at 4 °C under gentle agitation followed by three washes with buffer B (50 mM Tris-HCl, 200 mM NaCl, 10% glycerol, and 20 mM imidazole, pH 7.5). The proteins were eluted with buffer E (50 mM Tris-HCl, 200 mM NaCl, 10% glycerol, and 150 mM imidazole, pH 7.5). Eluted fractions were analyzed by SDS-PAGE, pooled, and dialyzed overnight against 1 liter of buffer D (50 mM Tris-HCl, 100 mM NaCl, 10% glycerol, 1 mM DTT, 1 mM $MgCl_2$, pH 7.5) and stored at −20 °C. Note that all Wzc_{CD} (or mutants thereof) preparations produced as described above resulted in species with a heterogeneously phosphorylated YC (data not shown) in line with that observed for Etk (18) and CapB (20).

Expression and Purification of Wzb Constructs Used for Enzymatic Assays—The DNA fragment encoding *wzb* and the mutants wzb_{C9S}, wzb_{L40A}, wzb_{Y117A}, and the double mutant $wzb_{L40A/Y117A}$ were PCR-amplified using either the pQE30-Wzb plasmid (38) or pQE30-Wzb_{L40A} plasmid (created for this study; for the double mutant only) and cloned into a pQE30 vector between the BamHI and Acc65I restriction sites. These mutants bearing N-terminal His_6 tags were produced in *E. coli* Xl1-blue cells and grown in LB medium supplemented with ampicillin and tetracycline. The overexpression and purification protocol was identical to that described for Wzc_{CD} (and variants) above.

Wzc_{CD} C-tail Peptides—Peptides derived from the C-terminal tail of Wzc_{CD} were custom-synthesized and HPLC-purified by Peptide2.0. These peptides included (i) WTpep (^{705}YQD**Y**G**YY**E**Y**E**Y**KSDAK^{720}) (phosphorylatable tyrosine residues are shown in boldface type); (ii) MUTpep (^{705}YQD**E**-G**EE**E**EE**E**E**KSDAK^{720}, where the phosphorylatable tyrosine residues in WTpep were mutated to glutamate in order to mimic the charge state of a phosphorylated tyrosine residue; (iii) PHOSpep (^{712}EY*E^{714}, where Y* represents 4-phosphomonomethylphenylalanine, a non-cleavable phosphotyrosine analog) (46). This peptide was chosen in order to test the affinity of Wzb for a singly phosphorylated species that would be a true mimic of phosphotyrosine and yet would not be cleaved by the enzymatic activity of Wzb.

Surface Plasmon Resonance Measurements—Analyses of the interactions between the different Wzc_{CD} and Wzb constructs were performed using surface plasmon resonance (SPR) using a BIAcore X100 (GE Healthcare). All experiments were performed at 25 °C. The buffers for the SPR measurements were filtered through 0.22-μm filters and degassed extensively before use. CM5 (carboxymethylated dextran; GE Healthcare) sensor chips were covalently coated with each of the three ligands Wzc_{CD}, $Wzc_{CD\Delta C}$, and $Wzc_{CD,ERR/A}$ (theoretical pI 8.9, 9.39, and 8.73, respectively). The ligands were dissolved to final concentrations of 21 μg/ml in 10 mM sodium acetate (pH 5.3) and immobilized onto CM5 chips by amine coupling on flow cells 2 (FC2), yielding responses of 951.2, 1512.8, and 490.8 for Wzc_{CD}, $Wzc_{CD\Delta C}$, and $Wzc_{CD,ERR/A}$, respectively, after deactivation of the CM5 surface with ethanolamine-HCl. As control, flow cells 1 (FC1) were activated for amine coupling and deactivated under the same conditions as FC2 in the absence of ligand.

The analytes, Wzb and Wzb_{C9S}, were diluted in a buffer containing 50 mM phosphate, 137 mM NaCl, 2.7 mM KCl, 25 mM DTT, 5 mM EDTA, and 0.005% P20-surfactant at pH 7.4 (SPR buffer), to reach final concentrations ranging from 100 nM to 10 μM. Each experiment consisted of three cycles where only the SPR buffer was passed over the CM5 sensor chip, followed by 11 cycles of different analyte concentrations (with one in duplicate). In each cycle, 50 μl of SPR buffer was injected first to stabilize the base line, followed by injection of the analyte (0–10 μM) through the two flow cells at 30 μl/min for 180 s. Responses detected on FC1 were considered to result from nonspecific binding and subtracted from the binding traces before detailed analyses. Dissociation of the bound analyte was achieved by passing SPR buffer over the two flow cells at 30 μl/min for 600 s. After the dissociation phase, a solution containing 5 M NaCl and 4 M $MgCl_2$ and another containing 10 mM triethylamine (10 μl/min for 60 s for each) were used to regenerate the CM5-ligand surface. Each experiment was recorded in duplicate, and reproducible signals were detected for every ligand-analyte pair tested.

FIGURE 1. **BY-kinases.** *A*, sequence alignment for BY-kinases. The conserved BY-kinase sequence motifs are indicated. The location of the α2 helix is shown by the *horizontal black line*, and the location of the E*XXR*X*X*R motif is shown by the *yellow rectangle* with the conserved residues (Glu, Arg, Arg) indicated by the *asterisks*. This alignment of BY-kinase sequences was used to generate Fig. 6*C*. *B*, structure of Wzc_{CD} (Protein Data Bank code 3LA6) (19). Conserved structural elements are *colored*, and the side chains of conserved residues are shown in *stick representations* and labeled. The characteristic BY-kinase motifs (conserved residues are shown in *boldface type*) for Wzc_{CD} are Walker A (^{533}**G**VSPSI**GKT**^{541}; *red*), Walker A′ (^{558}VLLI**D**C**D**M**R**^{566}; *orange*), and Walker B (^{639}VLI**D**TP**P**^{645}; *blue*). Also shown are helix α2, containing the conserved ^{508}**E**AI**R**SL**R**^{514} motif (*yellow*); the RK-cluster (Ser^{473}–Leu^{496}, *magenta*) (only Lys^{477} and Lys^{479} are seen in the crystal structure), and the C-tail (*green*; the YC tyrosines (Tyr^{705}, Tyr^{708}, Tyr^{710}, Tyr^{711}, Tyr^{713}, and Tyr^{715}) are shown). The Wzc_{CD} orientations are the same as in Fig. 6.

A

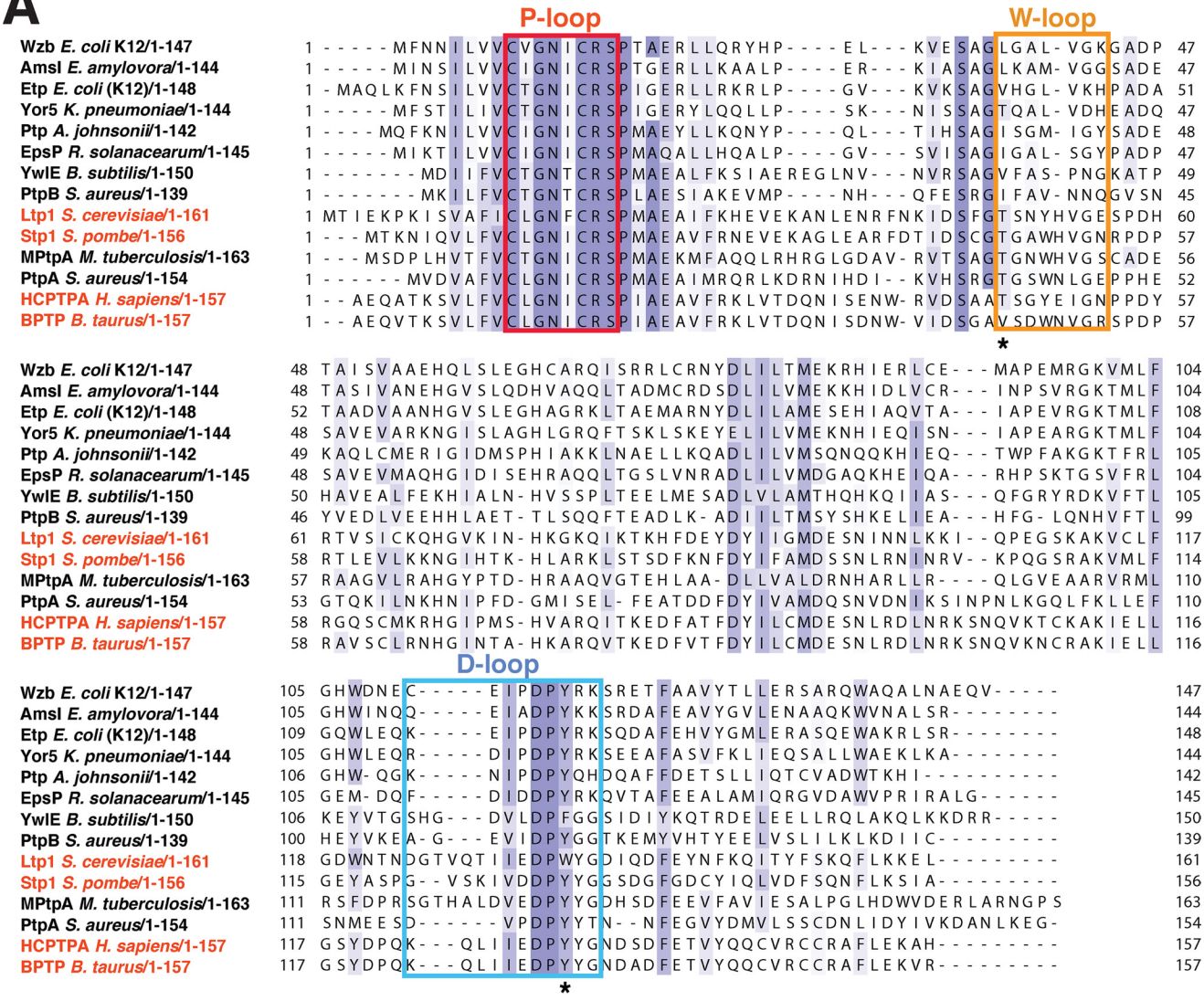
P-loop
W-loop
D-loop
Wzb E. coli K12/1-147
AmsI E. amylovora/1-144
Etp E. coli (K12)/1-148
Yor5 K. pneumoniae/1-144
Ptp A. johnsonii/1-142
EpsP R. solanacearum/1-145
YwlE B. subtilis/1-150
PtpB S. aureus/1-139
Ltp1 S. cerevisiae/1-161
Stp1 S. pombe/1-156
MPtpA M. tuberculosis/1-163
PtpA S. aureus/1-154
HCPTPA H. sapiens/1-157
BPTP B. taurus/1-157

B

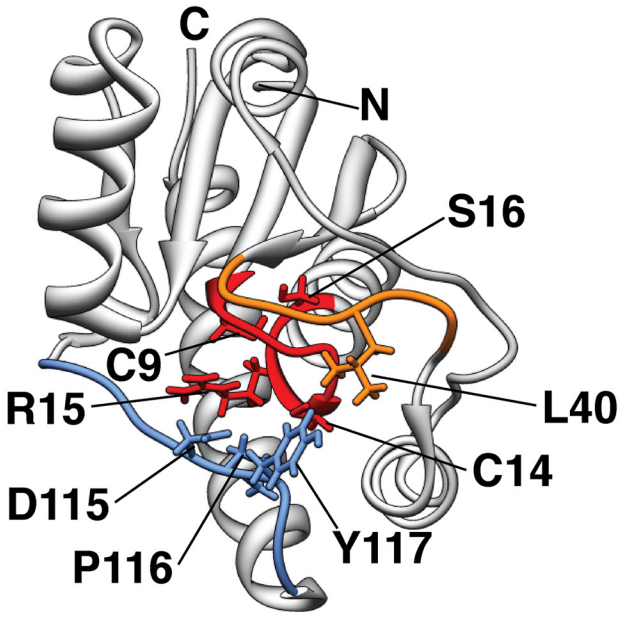
C
N
S16
C9
R15
L40
C14
D115
Y117
P116

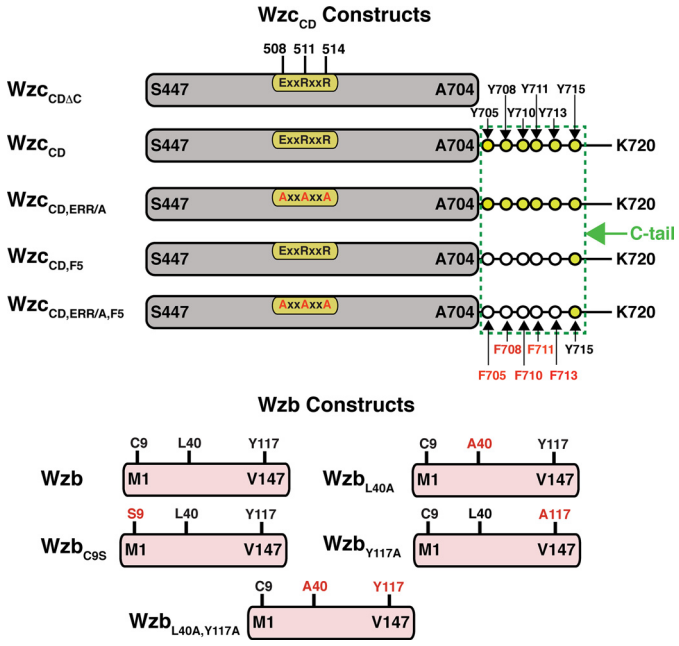

FIGURE 3. **Schematic representation of various Wzc$_{CD}$ and Wzb constructs used in this study.** The C-terminal tail (Tyr^{705}–Lys^{720}) is shown as a *green dashed box*. The tyrosine residues (*yellow filled circles*) belonging to the YC are labeled. Residues in the wild-type protein are labeled in *black*, and the corresponding residues in the mutated protein(s) are labeled in *red*. The YC tyrosine residues that are mutated to phenylalanine are indicated by *open circles*.

Transformation of experimental data were performed with the BIA-Evaluation software (GE Healthcare). No detailed kinetic analysis was performed for any of the sensorgrams, and equilibrium analysis to yield affinity values was performed for the Wzc$_{CD\Delta C}$ (ligand)/Wzb$_{C9S}$ (analyte) pair (also for the Wzc$_{CD}$/Wzb$_{C9S}$ pair at lower analyte concentrations) for which visual inspection of the sensorgrams confirmed 1:1 Langmuir-type binding. For these sensorgrams, the base line-subtracted ΔRU values were related to the concentration of analyte ($C_{analyte}$) and fitted to Equation 1 to obtain a K_d. The fits were performed using in-house software that utilized the ODRPACK subroutines (47).

$$\Delta RU = \frac{\Delta RU_{max}\, C_{analyte}}{K_d + C_{analyte}} \qquad \text{(Eq. 1)}$$

NMR Resonance Assignment—NMR samples used for resonance assignment were typically 300 μM protein (Wzc$_{CD}$, Wzc$_{CD\Delta C}$, and Wzb) in a buffer containing 50 mM phosphate, 50 mM NaCl, 25 mM DTT, 5 mM EDTA at pH 6.0 (NMR buffer). NMR experiments were carried out at 25 °C using Bruker Avance (600-, 700-, 800-, or 900-MHz), or Varian Innova (600-MHz) spectrometers equipped with cryogenic probes capable of applying pulse-field gradients along the z axis. NMR data were processed using NMRPipe (48) and analyzed using NMRViewJ (49).

The experimental methodology used for backbone resonance assignments of Wzc$_{CD}$ has been described in detail elsewhere (45). Backbone resonance assignments for Wzc$_{CD\Delta C}$ were obtained using TROSY-based (in all cases) HNCO/HN(CA)CO (512, 32, and 40 complex points with sweep widths of 13.35, 30, and 13 ppm in ^{1}H, ^{15}N, and ^{13}C dimensions, respectively); a HNCA/HN(CO)CA pair (512, 32, and 50/40 complex points with sweep widths of 13.35, 30, and 30 ppm in the ^{1}H, ^{15}N, and ^{13}C dimensions, respectively); and a HNCACB/HN(CO)CACB pair (512, 32, and 40/42 complex points with sweep widths of 13.35, 30, and 65 ppm in ^{1}H, ^{15}N, and ^{13}C dimensions, respectively) (50). No significant chemical shift changes were seen in the core residues of Wzc$_{CD}$ due to tail truncation (to generate Wzc$_{CD\Delta C}$). Additionally, eight resonances corresponding to the 21-residue N-terminal tag (that includes 6 histidines) were also assigned, and these resonances showed no significant differences in their positions between Wzc$_{CD}$ and Wzc$_{CD\Delta C}$ or for each species in the presence of Wzb. The corresponding tag in Wzb was also unaffected in the presence of Wzc$_{CD}$ or Wzc$_{CD\Delta C}$.

Nearly complete ^{15}N, ^{13}C, and ^{1}H resonance assignments for full-length Wzb are available from Lescop *et al.* (34). However, due to some differences under our conditions, the assignments of several of these resonances needed to be confirmed. Non-uniformly sampled versions of HNCO/HN(CA)CO (512, 32, and 50 complex points with sweep widths of 13, 32, and 13 ppm in ^{1}H, ^{15}N, and ^{13}C dimensions, respectively); HNCACB/CBCA(CO)NH (512, 32, and 50 complex points with sweep widths of 13, 32, and 65 ppm in ^{1}H, ^{15}N, and ^{13}C dimensions respectively); and HNCA/HN(CO)CA (512, 32, and 50 complex points with sweep widths of 10, 32, and 30 ppm in ^{1}H, ^{15}N, and ^{13}C dimensions, respectively) were collected using a 30% sampling schedule generated by the *sparse.py* script (51). All data were collected at 700 MHz and 25 °C and reconstructed using MDDGui software (52).

^{13}C,^{1}H resonance assignments for the aromatic side chains of Wzb were obtained using (Hβ)Cβ(CγCδ)Hδ, (Hβ)Cβ(CγCδCϵ)Hϵ (512 and 40 complex points with sweep widths of 12 and 30 ppm in ^{1}H and ^{13}C dimensions, respectively) (53) and ^{13}C-edited NOESY-HSQC (512, 40, and 88 complex points with sweep widths of 12, 30, and 12 ppm in the ^{1}H, ^{13}C, and ^{1}H dimensions, respectively) experiments at 700 MHz and 25 °C. A mixing time of 120 ms was used for the ^{13}C-edited NOESY-HSQC experiment.

NMR Titrations to Determine Wzc$_{CD}$/Wzb Interactions—Chemical shift perturbations in 100 μM uniformly ^{15}N,^{2}H-labeled Wzc$_{CD}$ or Wzc$_{CD\Delta C}$ (in NMR buffer, described above) were obtained by separate titration sets with ^{2}H-labeled Wzb at concentrations of 25, 50, 75, and 100 μM, and ^{15}N,^{1}H TROSY spectra were acquired at each titration point. Similarly, 100 μM uniformly ^{15}N,^{2}H-labeled Wzb (in NMR buffer) was titrated with either uniformly ^{2}H-labeled Wzc$_{CD\Delta C}$ or uniformly ^{2}H-la-

FIGURE 2. **Low molecular weight protein tyrosine phosphatases (LMW-PTPs).** *A*, sequence alignment for LMW-PTPs. Sequences for eukaryotic LMW-PTPs are shown in *red*. Locations of the P-loop, D-loop, and W-loop are indicated. The Leu^{40} (W-loop) and Tyr^{117} (D-loop) positions in *E. coli* (K12) Wzb are indicated by the *asterisks*. The alignment of LMW-PTP sequences was used to generate Fig. 7*C*. *B*, structure of Wzb (Protein Data Bank code 2FEK) (34). The P-loop is *colored red* (**C**VGNI**CRS**), the D-loop (with the conserved DPY) sequence shown in a *stick representation*) is *colored blue*, and the W-loop (Leu^{40} is shown in a *stick representation*) is *colored orange*. The Wzb orientation is the same as in the extreme *right-hand panels* of Fig. 7, *A–C*.

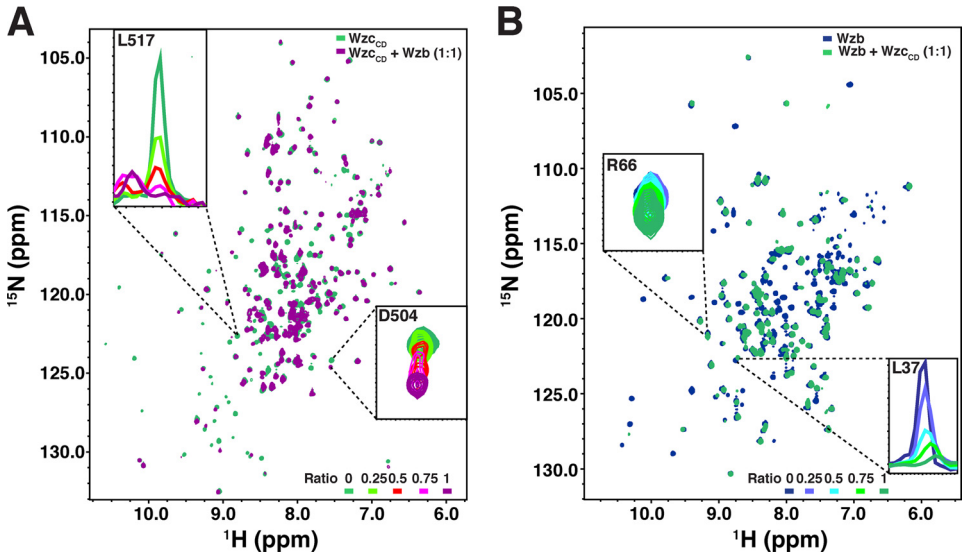

FIGURE 4. **Representative spectra for the NMR-based titration sets.** *A*, spectral changes in ^{15}N,^{1}H TROSY spectra (800 MHz) of uniformly ^{15}N,^{2}H-labeled Wzc$_{CD}$ in the presence of an equimolar amount of uniformly ^{2}H-labeled Wzb. *B*, spectral changes in ^{15}N,^{1}H TROSY spectra (800 MHz) of uniformly ^{15}N,^{2}H-labeled Wzb in the presence of an equimolar amount of uniformly ^{2}H-labeled Wzc$_{CD}$. The *insets* in each case depict representative examples of chemical shift and intensity changes during the course of the titrations (*i.e.* in the presence of increasing amounts of Wzb (*A*) or Wzc$_{CD}$ (*B*)). The molar ratios of the titrant are indicated in the *bottom right* in each case.

beled Wzc$_{CD}$ at concentrations of 25, 50, 75, and 100 μM, and ^{15}N,^{1}H TROSY spectra were recorded for each titration point. All spectra were acquired at 900 MHz and 25 °C using sweep widths of 13.35 ppm (512 complex points) and 30 ppm (128 complex points) in the ^{1}H and ^{15}N dimensions, respectively. Recycle delays of 1.5 s were used, and 16 transients were collected per t_1 point. Representative spectra corresponding to the various NMR-based titrations involving Wzc$_{CD}$ and Wzb are shown in Fig. 4. As can be seen, the spectra are of excellent quality.

Note that for all NMR-based titrations and spin relaxation experiments (described below), the last titration point contained an equimolar ratio of Wzc$_{CD}$ (or Wzc$_{CD\Delta C}$) and Wzb for a total protein concentration of 200 μM. Assuming a K_d of ~2–5 μM, we would expect ~80–85% of the proteins to be in the complexed state. We did not use higher total protein concentration (*i.e.* saturating equivalents) to ensure sample stability during the measurements. However, no significant additional perturbations, compared with those at the equimolar ratio, were seen in the presence of saturating amounts of ligand at lower concentrations of the species being probed.

NMR Titrations to Determine Wzb/Phosphate Interactions—A series of ^{15}N,^{1}H HSQC spectra were recorded using 100 μM ^{13}C,^{15}N-labeled Wzb, each with an incremental amount of potassium phosphate to obtain the following Wzb/phosphate ratios: 1:2, 1:3, 1:5, 1:10, 1:20, 1:40, 1:100, and 1:200. Titrations were performed in a buffer containing 20 mM BisTris, 50 mM NaCl, 25 mM DTT at pH 6.0 (BT buffer). The initial volume of 350 μl increased to 363.5 μl at the end of the addition, resulting in a dilution of less than 4%. All spectra were recorded at 600 MHz at 25 °C using sweep widths of 13 ppm (512 complex points) and 32 ppm (128 complex points) for the ^{1}H and ^{15}N dimensions, respectively.

NMR Titrations to Determine Wzb/C-tail Peptide Interactions—The WTpep, MUTpep, and PHOSpep peptides were titrated into 100 μM ^{15}N-labeled Wzb in BT buffer to the following final concentrations: 0, 200, and 400 μM. Individual samples were made for each of the Wzb-WTpep, Wzb-MUTpep and Wzb-PHOSpep complexes, and the following spectra were acquired: ^{15}N,^{1}H HSQC (512 and 128 complex points with sweep widths of 13 and 32 ppm in the ^{1}H and ^{15}N dimensions, respectively), constant time ^{13}C,^{1}H HSQC optimized for the aromatic region (512 and 64 complex points with sweep widths of 12 and 30 ppm in the ^{1}H and ^{13}C dimensions, respectively), and ^{13}C,^{1}H HSQC optimized for the methyl region (512 and 115 complex points with sweep widths of 12 and 20 ppm in the ^{1}H and ^{13}C dimensions, respectively). Only ^{15}N,^{1}H HSQC spectra were recorded for the Wzb-MUTpep complexes. All spectra were recorded at 800 MHz and 25 °C.

In all NMR-based titrations, chemical shift perturbations ($\Delta\delta_i$) or signal attenuations (ΔI_i) for each residue at each titration point (indexed by i) were calculated using the following equations.

$$\Delta\delta_i = \sqrt{(\Delta\delta_{0,H} - \Delta\delta_{i,H})^2 + 0.11(\Delta\delta_{0,N} - \Delta\delta_{i,N})^2} \quad \text{(Eq. 2)}$$

$$\Delta I_i = 1 - \frac{I_i}{I_0} \quad \text{(Eq. 3)}$$

The 0 subscript indexes the ^{1}H/^{15}N chemical shifts (δ) or the intensities (I) for the reference state (no ligand present).

Spin Relaxation Measurements—TROSY-based relaxation experiments to obtain spin-spin relaxation rates (R_2) (54) were recorded at 800 MHz and 25 °C for Wzc$_{CD}$, Wzc$_{CD\Delta C}$, and Wzb and for their equimolar mixtures. Samples typically were 100 μM protein in NMR buffer, with the equimolar mixtures containing a 100 μM concentration of each of the constituent proteins. Samples used (and relaxation delays) are provided in Table 1. Relaxation data were acquired with sweep widths of 13.35 ppm (512 complex points) and 30 ppm (128 complex points) in the ^{1}H and ^{15}N dimensions, respectively, for Wzc$_{CD}$,

TABLE 1

Measurement of ^{15}N spin-spin relaxation rates (R_2)

R_2 data were measured for the species in boldface type. All experiments were performed at 800 MHz and 25 °C. Complexes contained an equimolar ratio of the two proteins.

Sample	Relaxation delay
	ms
$^{15}N,^{2}H$-Labeled Wzc_{CD}	0, 16, 33, 49, 65, 82
$^{15}N,^{2}H$-Labeled Wzc_{CD} + ^{2}H-labeled Wzb	0, 16, 33, 33, 49
$^{15}N,^{2}H$-Labeled $Wzc_{CD\Delta C}$	0, 16, 33, 49, 65, 82
$^{15}N,^{2}H$-Labeled $Wzc_{CD\Delta C}$ + ^{2}H-labeled Wzb	0, 16, 33, 49, 65
$^{15}N,^{2}H$-Labeled Wzb	0, 16, 33, 49, 65, 98, 131, 163
$^{15}N,^{2}H$-Labeled Wzb + ^{2}H-labeled $Wzc_{CD\Delta C}$	0, 16, 33, 49, 65, 82
$^{15}N,^{2}H$-labeled Wzb + ^{2}H-labeled Wzc_{CD}	0, 16, 33, 49, 65

$Wzc_{CD\Delta C}$, and their equimolar mixtures with Wzb and with sweep widths of 13 ppm (512 complex points) and 30 ppm (128 complex points) in the ^{1}H and ^{15}N dimensions, respectively, for Wzb and for its equimolar mixtures with Wzc_{CD} and $Wzc_{CD\Delta C}$.

Enzymatic Assays—400 μg of Wzc_{CD} (or the corresponding mutant proteins: $Wzc_{CD,ERR/A}$, $Wzc_{CD,F5}$, and $Wzc_{CD,F5,ERR/A}$) was incubated in the presence of 20 μCi of radioactive [γ-^{32}P]ATP (3000 Ci/μmol) and 25 μM non-radioactive ATP in a buffer containing 25 mM Tris-HCl, 5 mM $MgCl_2$, 1 mM EDTA, 1 mM DTT at pH 7.5 for 30 min at 37 °C. This was followed by extensive dialysis in the same buffer to remove radioactive ATP, followed by dephosphorylation using Wzb. For dephosphorylation, Wzc_{CD} (or $Wzc_{CD,ERR/A}$, or $Wzc_{CD,F5}$, or $Wzc_{CD,F5,ERR/A}$) and Wzb were mixed in a buffer containing 100 mM sodium citrate and 1 mM EDTA at pH 6.5 and incubated for a series of times (0, 1, 2, 5, 10, 20, and 30 min) at 37 °C using several kinase/phosphatase molar ratios (5:1, 10:1, 20:1, 25:1, 30:1, and 35:1) with the quantity of Wzb being fixed at 2.85 pmol (in a reaction volume of 128 μl corresponding to a concentration of 22.3 nM). Negative controls for the same times were performed in the absence of Wzb (data not shown). Samples were analyzed by SDS-PAGE and autoradiography. Bands corresponding to radioactive Wzc_{CD} (or $Wzc_{CD,ERR/A}$, or $Wzc_{CD,F5}$, or $Wzc_{CD,F5,ERR/A}$) were cut out from the gels and dissolved in 400 μl of 30% hydrogen peroxide and 200 μl of 60% perchloric acid for 4 h at 80 °C. After the addition of 10 ml of scintillation liquid (ULTIMA GOLD™ XR), the radioactivity was measured in a scintillation counter (Tri Carb 2100 TR, Packard). The cpm values were then converted to pmol of phosphate remaining on $Wzc_{CD,F5}$ (or $Wzc_{CD,F5,ERR/A}$). Michaelis-Menten parameters (V_{max} and K_m were estimated using Hanes-Woolf representations (Equation 4). Data analysis was carried out using in-house programs that utilize the ODRPACK (47) subroutines.

$$\frac{C_{substrate}}{V} = \frac{1}{V_{max}} C_{substrate} + \frac{K_M}{V_{max}} \quad \text{(Eq. 4)}$$

To test the activity of the mutant Wzb proteins, γ-^{32}P-labeled Wzc_{CD} (generated as described above) was incubated for 10 or 25 min in the absence or presence of either Wzb, Wzb_{C9S}, Wzb_{L40A}, Wzb_{Y117A}, or $Wzb_{L40A,Y117A}$. The mixtures were then analyzed by SDS-PAGE, and the extent of Wzc_{CD} dephosphorylation was ascertained using direct film exposure and scintillation counting as described above.

RESULTS

In Vitro Interaction between Wzc_{CD} and Wzb—As a first step toward detailed characterization of the interaction between Wzc_{CD} and Wzb, we used SPR to estimate the affinity of their association. In all cases, we used Wzc_{CD} (or mutants thereof; see Fig. 3 for the various Wzc and Wzb constructs used in this study) as a ligand affixed onto the sensor chip surface and Wzb (or mutants thereof; see Fig. 3) as an analyte. First, in order to test whether the C-tail of Wzc_{CD} bearing the YC (the phosphorylated YC being the natural substrate of Wzb) is necessary for the Wzc_{CD}/Wzb interaction, we used a Wzc_{CD} construct missing the C-tail ($Wzc_{CD\Delta C}$) as ligand. The sensorgram (Fig. 5*A*) for the $Wzc_{CD\Delta C}$/Wzb interaction was biphasic, especially at higher analyte concentrations, suggesting deviations from a simple 1:1 Langmuir-type binding, making it inappropriate for an equilibrium analysis. The curvature of the association stage of the sensorgram was not sufficient (fast association) for a meaningful kinetic analysis; therefore, such an analysis was not attempted for this (or for any other) case. However, when a catalytically inactive mutant of Wzb (Wzb_{C9S}; where Cys^9, the catalytic cysteine nucleophile, is replaced by serine) (Fig. 3) was used as the analyte, a Langmuir-type behavior (Fig. 5*B*) was obtained (for the $Wzc_{CD\Delta C}$/Wzb_{C9S} interaction), and an equilibrium analysis yielded a K_d value of 5.1 ± 0.2 μM. Sensorgrams corresponding to Wzc_{CD}/Wzb (Fig. 5*C*) and Wzc_{CD}/Wzb_{C9S} (Fig. 5*D*) interactions were highly biphasic, displaying a second slow process following the initial fast association. An equilibrium analysis (data not shown) of the Wzc_{CD}/Wzb_{C9S} sensorgram at lower analyte concentrations where the non-Langmuir behavior is less pronounced (for analyte concentration below 5.0 μM) yielded a K_d of 2.3 ± 0.4 μM, comparable with that obtained for the $Wzc_{CD\Delta C}$/Wzb_{C9S} interaction. Overall, our analysis suggests that a region on Wzc_{CD} distinct from the phosphorylated C-tail provides a majority of the binding energy for the Wzc_{CD}/Wzb interaction.

Binding Site of Wzb on Wzc_{CD}—Next, we attempted to ascertain specific residues on Wzc_{CD} that interact with Wzb, using solution NMR techniques. Taking cue from the SPR results that showed that the YC of Wzc_{CD} did not play a significant role in binding, we analyzed the spectral perturbations induced on a $^{1}H,^{15}N$ TROSY spectrum of $^{15}N,^{2}H$-labeled $Wzc_{CD\Delta C}$ in the presence of an equimolar ratio of full-length, uniformly ^{2}H-labeled Wzb. In addition to the uniform broadening of $Wzc_{CD\Delta C}$ resonances due to complex formation, resulting in an increase in overall molecular mass (^{15}N R_2 for apo = 26.4 ± 5.9 s^{-1}, indicative of a monomer in solution; ^{15}N R_2 in the presence of Wzb at a 1:1 ratio = 41.0 ± 11.2 s^{-1}, indicating complex formation; data at 800 MHz with 100 μM $Wzc_{CD\Delta C}$), specific chemical shift changes and selective resonance attenuation were seen. The largest chemical shift changes were seen on the N terminus of α1 and the C terminus of α3. Some smaller but significant changes were also seen on αA and β7. However, an analysis of the selective signal attenuation (indicative of exchange on the intermediate time scale) was far more informative. Resonances corresponding to all of α2 and most of βA, β1, β6, and β7 were completely broadened out in the presence of Wzb. As shown in Fig. 6A, the residues that display chemical

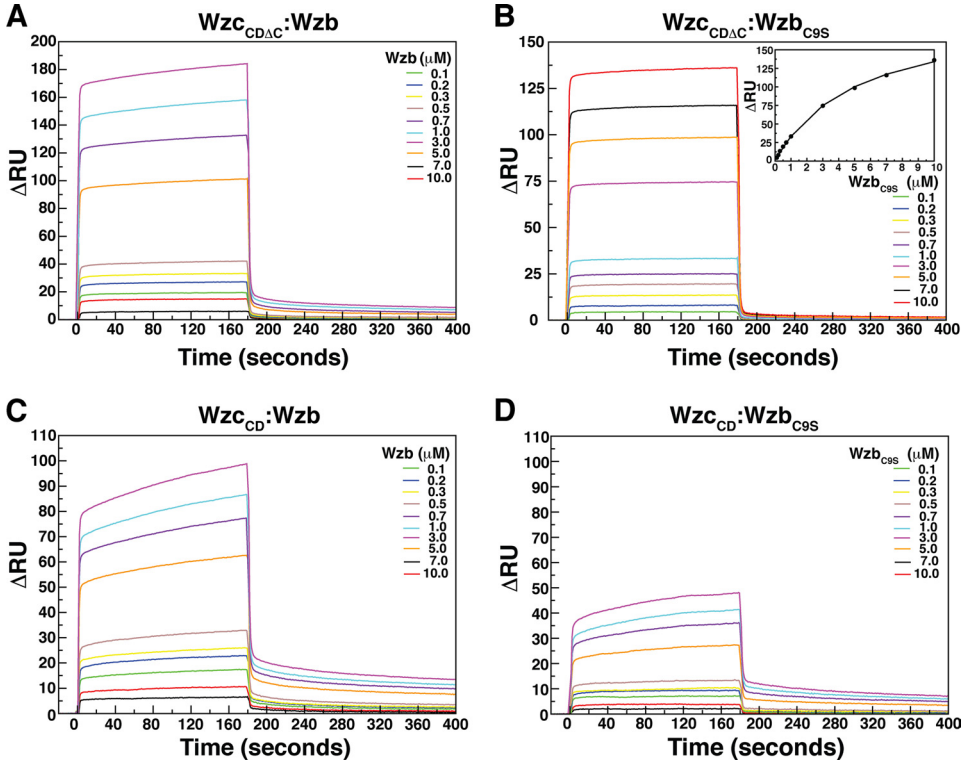

FIGURE 5. **SPR analysis of the interactions of Wzc_{CD} with Wzb.** Sensorgrams corresponding to the interaction of $Wzc_{CD\Delta C}$ (*A* and *B*) or Wzc_{CD} (*C* and *D*) at varying concentrations of wild-type Wzb (*A* and *C*) or the catalytically dead mutant of Wzb (Wzb_{C9S}; *B* and *D*) are shown. In all cases, the Wzc_{CD} constructs (ligands) were affixed onto the sensor chip surface, and the Wzb constructs were used as analytes. The *inset* in *B* depicts the result of the equilibrium analysis for the $Wzc_{CD\Delta C}$/Wzb_{C9S} interactions. Experimental data are shown as *circles*, and the theoretical curve corresponding to a 1:1 binding model is shown as a *solid line*.

shift changes and selective attenuation form a continuous surface on the face opposite to that hosting the catalytic site of Wzc. In fact, no significant spectral perturbations (chemical shift changes or loss of signals) were observed at the active site. Note that ^{15}N,^{1}H resonances other than those belonging to the Walker B motif are largely assigned for the active site (45).

In order to obtain additional insight into the spectral perturbations, we analyzed a TROSY spectrum of $Wzc_{CD\Delta C}$ in the presence of substoichiometric amounts of Wzb (1:0.25, the first point in our titration course, 1:1 being the last). In this case (*i.e.* for a $Wzc_{CD\Delta C}$/Wzb ratio of 1:0.25), although no significant chemical shift changes were seen (except for Ile^{510}; 0.19 ppm), resonances corresponding to almost all of α2 (Ala^{506}, Ala^{509}, Arg^{511}, Ser^{512}, Leu^{513}, Arg^{514}, Ala^{520}, and Met^{521}) were broadened to below the noise level (average attenuation for α2 = 0.80 ± 0.23, compared with 0.35 ± 0.29 for all resonances). Complete attenuation of some other resonances (Tyr^{467}, Ile^{470}, Leu^{547}, Leu^{663}, Ala^{666}, Ile^{694}, and Leu^{695}) was seen. Notably, the side chains of these residues lie in close spatial proximity to α2, suggesting the importance of α2 in Wzc/Wzb interactions. NMR titrations with Wzc_{CD} produced similar results (Fig. 6*B*), again with α2 and spatially proximal regions displaying the largest specific spectral perturbations. α2 shows a degree of sequence conservation that is the highest outside the catalytic site (see Fig. 6*C*; also see Fig. 1*A*). Notably, α2 contains the conserved ^{508}E*XX*R*XX*R^{514} that was discussed at length in the Introduction. It therefore appears that the Wzb docking site on Wzc_{CD} overlaps with that shown to play a role in the oligomerization and consequent trans-phosphorylation of the latter.

As expected from the SPR results, minimal spectral perturbations were seen for the YC of Wzc_{CD}. Note that the species probed by the NMR experiments (unlike the SPR results that involved the catalytically dead Wzb_{C9S} mutant) corresponds to the dephosphorylated YC. Given the efficiency of Wzb, the dephosphorylation reaction was almost complete before any NMR data could be recorded (>90% dephosphorylated in 30 min at a 1:1 ratio; data not shown). Nevertheless, some attenuations were seen in the YC, including for Tyr^{708} (0.52), Glu^{714} (fully attenuated), and Tyr^{715} (0.55). It is possible that this weak interaction of the dephosphorylated C-tail of Wzc_{CD} with Wzb was the cause of the second slow association event seen in the SPR analysis of Wzc_{CD}/Wzb interactions. However, as will be shown, the isolated dephosphorylated C-tail of Wzc_{CD} does not bind Wzb in *trans*. The weak association seen here is due to its elevated local concentration as a result of the docking interaction of Wzb with the putative oligomerization surface of Wzc_{CD} described above. This is also the likely mechanism for substrate (*i.e.* phospho-YC recognition), as discussed below.

Binding Site of Wzc_{CD} on Wzb—As expected, an overall decrease in signal intensity was seen in the ^{15}N,^{1}H TROSY spectrum of uniformly ^{15}N,^{2}H-labeled Wzb in the presence of an equimolar amount of uniformly ^{2}H-labeled $Wzc_{CD\Delta C}$ (or ^{2}H-labeled Wzc_{CD}) due to an increase in the molecular mass in solution (^{15}N R_2 for free Wzb = 15.6 ± 4.1 s^{-1}; ^{15}N R_2 in the presence of a 1:1 ratio of $Wzc_{CD\Delta C}$ = 31.0 ± 5.6 s^{-1}; ^{15}N R_2 in the presence of a 1:1 ratio of Wzc_{CD} = 41.9 ± 9.6 s^{-1}; 800 MHz, 100 μM Wzb). In addition, selective perturbations indicative of specific interaction, were seen covering almost an entire face

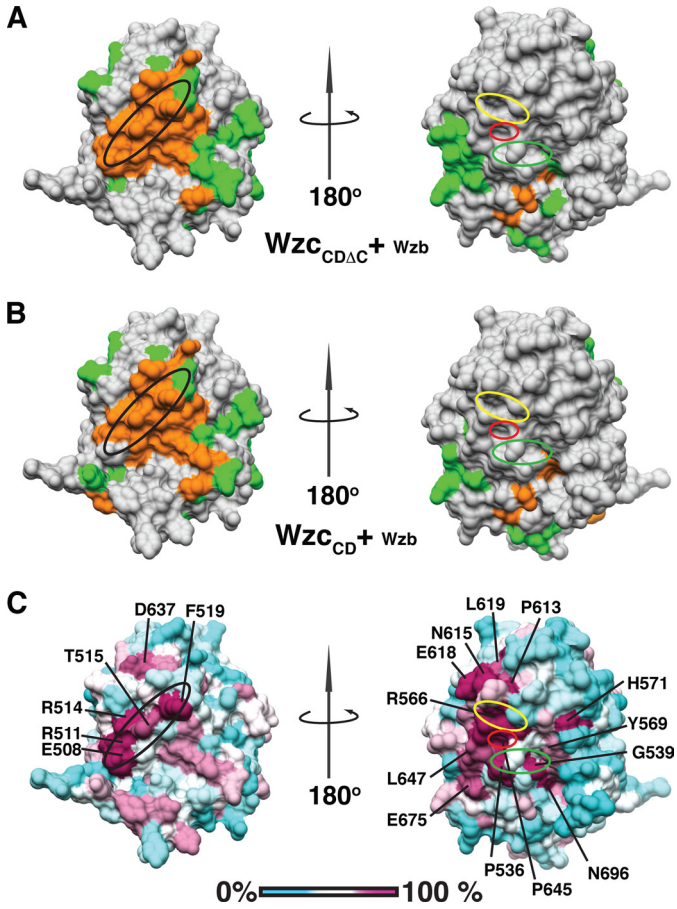

FIGURE 6. **Analysis of perturbations in Wzc$_{CD}$ (or Wzc$_{CD\Delta C}$) spectra in the presence of Wzb.** Shown are perturbations in the ^{15}N,^{1}H TROSY spectra of uniformly ^{2}H,^{15}N-labeled Wzc$_{CD\Delta C}$ (*A*) or Wzc$_{CD}$ (*B*) in the presence of an equimolar ratio of uniformly ^{2}H-labeled Wzb, mapped onto the Wzc$_{CD}$ surface (Protein Data Bank code 3LA6; species probed shown in *larger type*). Residues that display chemical shift changes greater than the mean + 2 S.D. (0.036 ppm for Wzc$_{CD\Delta C}$; 0.044 ppm for Wzc$_{CD}$) are *colored green*; residues that are broadened to below the noise level are *colored orange*. *C*, sequence conservation (also see Fig. 1*A*) in the CDs of BY-kinases plotted on the Wzc$_{CD}$ surface using a *cyan* (0% conservation) to *magenta* (100% conservation) gradient. The E*XXRXX*R (*black*), Walker A (*green*), Walker A′ (*yellow*), and Walker B (*red*) motifs are indicated by the *solid ovals*.

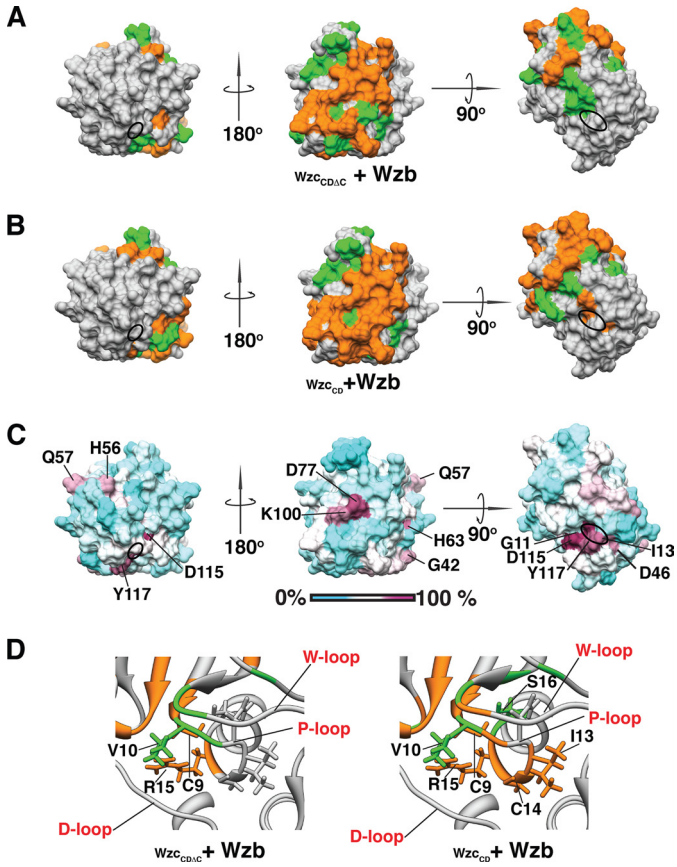

FIGURE 7. **Analysis of perturbations in Wzb spectra in the presence of Wzc$_{CD}$ (or Wzc$_{CD\Delta C}$).** Perturbations in the ^{15}N,^{1}H TROSY spectra of uniformly ^{2}H,^{15}N-labeled Wzb in the presence of equimolar ratios of uniformly ^{2}H-labeled Wzc$_{CD\Delta C}$ (*A*) or Wzc$_{CD}$ (*B*), mapped onto the Wzb surface (Protein Data Bank code 2FEK; species probed shown in *larger type*). Residues that display chemical shift changes greater than the mean + 2 S.D. (0.028 ppm in the presence of Wzc$_{CD\Delta C}$; 0.038 ppm in the presence of Wzc$_{CD}$) are *colored green*; residues that are broadened to below the noise level are *colored orange*. *C*, sequence conservation (also see Fig. 2*A*) in LMW-PTPs plotted on the Wzb surface using a cyan (0% conservation) to magenta (100% conservation) gradient. *D*, *close-up* of the Wzb active site in the presence of either Wzc$_{CD\Delta C}$ (*left*) or Wzc$_{CD}$ (*right*). Significant perturbations at the active site in the absence of substrate (*i.e.* the C-tail in the case of Wzc$_{CD\Delta C}$) indicate allosteric effects upon docking interactions. The P-loop and D-loop containing key catalytic site residues are labeled. Also labeled is the so-called W-loop that, in the case of Wzb, does not contain a tryptophan. Selected residues that depict significant spectral perturbations are shown in *stick representations* and *labeled*.

near the catalytic site of Wzb (Fig. 7). The patterns of perturbations seen in the spectra of Wzb in the presence of either Wzc$_{CD\Delta C}$ or Wzc$_{CD}$ were similar (Fig. 7, compare *A* and *B*). Overall, the magnitudes of the chemical shift perturbations were significantly smaller than those seen for Wzc$_{CD\Delta C}$ or Wzc$_{CD}$ in the presence of Wzb, and as in those cases, an analysis of the selective attenuations was far more informative. A majority of resonances corresponding to the N terminus of Wzb, β1, α3, β3, and α4 were broadened to below the noise level. Most significantly, many resonances corresponding to the so-called P-loop that contains the C*XXXXX*R(T/S) (^{9}**C**VGNI**CRS**^{16}) motif (Fig. 2), conserved in all Cys-based phosphatases (37), were significantly perturbed. However, a very interesting pattern emerged upon closer inspection of resonances corresponding to the P-loop of Wzb in the presence of Wzc$_{CD\Delta C}$ (Fig. 7*D*). Despite the absence of the YC in the Wzc$_{CD\Delta C}$ construct, significant spectral perturbations were noted at the catalytic site of Wzb. Residues that were broadened to below the noise level included the catalytic Cys^{9} (that carries out the initial nucleophilic attack on the phosphotyrosine moiety) and Arg^{15} (that stabilizes the transition state). Given that these changes occur in the absence of substrate (*i.e.* the phosphorylated YC of Wzc), they probably indicate allosteric effects at the Wzb active site upon docking interactions with Wzc$_{CD\Delta C}$ (this could also be the origin of the mildly biphasic behavior of the Wzc$_{CD\Delta C}$/Wzb sensorgram; see Fig. 5*A*). Additional perturbations, covering almost all of the P-loop (Fig. 7*D*), were seen in the presence of Wzc$_{CD}$. These results suggest a scenario in which docking interactions occur between Wzc$_{CD}$ and Wzb in a YC-independent manner, raising the local concentration of the YC, which then samples the active site of Wzb. This is consistent with the results obtained from the Wzc$_{CD}$ side, as described above.

Substrate Recognition by Wzb—Next, in order to ascertain the key determinants of substrate recognition by Wzb, we monitored changes in ^{15}N,^{1}H HSQC spectra of ^{15}N-labeled Wzb in

the presence of an increasing concentration of a 16-residue peptide (WTpep) corresponding to the dephosphorylated C-terminal tail (Tyr^{705}–Lys^{720}). Lack of any significant spectral perturbations (data not shown) confirmed the extremely low affinity in *trans* of the dephosphorylated C-tail of Wzc_{CD} for Wzb. Additionally, no significant spectral perturbations were seen in the presence of another 16-residue peptide (MUTpep; WTpep carrying a Y708E/Y710E/Y711E/Y713E/Y715E mutation to mimic the charge state of the fully phosphorylated YC). *In vivo* the YC has been found to be multiply phosphorylated (20, 23, 28), and this highly phosphorylated YC is the natural substrate of Wzb. It therefore follows that Wzb is capable of organizing several negative charges near its active site. Hence, that Wzb does not bind MUTpep is due to the fact that glutamate, although an excellent mimic for phosphoserine or phosphothreonine, is an extremely poor mimic for phosphotyrosine (55). However, significant spectral perturbations were seen in the presence of phosphate. A large number of chemical shift changes (>0.04 ppm; Fig. 8*A*) were seen emanating from the active site of Wzb in the presence of a 5-fold excess of phosphate. Interestingly, resonances corresponding to Cys^{9}, Val^{10}, Glu^{20}, Leu^{40}, and Tyr^{117} only appear in the presence of a large excess of phosphate (200-fold excess under our experimental conditions), whereas additional resonances corresponding to residues Gly^{11}, Ile^{13}, Cys^{14}, and Arg^{15} can only be seen in phosphate buffer. The appearance of additional resonances in the presence of phosphate has been noted by Lescop *et al.* (34) (Note that the titrations involving Wzc_{CD}, $Wzc_{CD\Delta C}$, and Wzb, described earlier were carried out in phosphate buffer; this was to allow the analysis of spectral perturbations for several resonances at the Wzb active site that are exchange-broadened and not observable in the absence of phosphate, as described above; see "Experimental Procedures"). It therefore appears that the phosphate moiety plays a significant role in substrate recognition by Wzb. It is to be noted that Wzb has no activity toward phosphoserine or phosphothreonine,[5] although selectivity toward phosphotyrosine is probably obtained in part by the depth of the catalytic cavity of Wzb (phosphoserine and phosphothreonine side chains are not long enough to reach the catalytic elements), and additional stabilization of the large hydrophobic tyrosine moiety near the active site is required for stable processing following phosphate recognition.

In order to ascertain the origin of the selectivity of Wzb toward phosphotyrosine, one would ideally use a peptide phosphorylated on a single tyrosine. However, such a phosphotyrosine peptide, being a natural substrate for Wzb, would be efficiently dephosphorylated before any NMR experiments could be conducted. Therefore, we monitored the spectral perturbations in Wzb in the presence of a tripeptide, EY*E (PHOSpep, where Y* represents 4-phosphomonomethylphenylalanine). The choice of this peptide incorporating an unnatural amino acid was guided by the fact that it truly mimics a phosphotyrosine (in a way that glutamate does not) in that it contains both a phosphate group and an aromatic ring. Additionally, being non-cleavable, it is stable under the enzymatic activity of Wzb. Despite the fact that the YC has been found to be multiply phosphorylated *in vivo*, as discussed earlier, the overall size of the Wzb catalytic cavity ensures that it cannot accommodate more than one phosphotyrosine at any given time, a condition that is effectively simulated by PHOSpep.

Unlike in the case of phosphate, where a large number of chemical shift changes were seen, suggesting chemical exchange on the fast time scale (as expected from a K_d value of 630 ± 118 μM obtained by fitting the chemical shift changes against phosphate concentration), PHOSpep generated significant changes in intensity without any major chemical shift changes. In addition, several peaks showed doubling, with one peak reducing in intensity and the other increasing in intensity with increasing PHOSpep concentration, indicative of slow exchange on the chemical shift time scale (Fig. 8*B*). Fitting the changes in intensity with PHOSpep concentration yields a K_d of 261 ± 65 μM, suggesting an affinity that is comparable with that seen for phosphate alone. This reinforces the fact the majority of the binding affinity of Wzc_{CD} for Wzb is provided by docking interactions that do not involve the YC. A point to note is that the slow exchange regime seen here, although unusual for the weak affinity, is however not unprecedented (56, 57). This apparent anomaly could be due to an unusual k_{on} or the result of a slow conformational change following the binding event. Here we analyze these effects only qualitatively in the context of YC recognition; a more detailed analysis, not relevant in the present context, is left for future studies. Overall, the spectral perturbations seen in Wzb in the presence of PHOSpep are similar to those seen with phosphate alone. However, PHOSpep induces a larger degree of spectral perturbations, in relative terms, on helix α5 of Wzb compared with phosphate (Fig. 8, compare *A* and *C*). This helix includes two aromatic residues, Phe^{124} (minimal perturbation, although the flanking residues Thr^{123} and Ala^{125} have attenuations of 0.40 and 0.46, respectively) and Tyr^{128} (attenuation = 0.43; in fact, the stretch between Tyr^{128} and Leu^{131} shows an average attenuation of 0.51), which are highly conserved in bacterial LMW-PTPs (see Fig. 2A). The perturbations in these regions and the suggestion that the D-loop Tyr^{117} contributes to substrate recognition open the possibility that a reorientation of α5 increases base-stacking interactions with the phosphotyrosine moiety. As stated earlier, the ^{15}N,^{1}H resonance corresponding to Tyr^{117} can only be seen at high phosphate concentration. In order to probe the role of Tyr^{117}, and possibly of Phe^{124} and Tyr^{128}, in substrate stabilization, we analyzed ^{13}C,^{1}H HSQC spectra, focusing specifically on the aromatic groups (Fig. 9*A*). The aromatic resonances corresponding to Phe^{124} were weak and could not be analyzed. However, significant attenuations were seen for the δ- and ϵ-resonances corresponding to Tyr^{117} in the presence of PHOSpep, although none of the resonances corresponding to Tyr^{128} displayed any significant perturbations. No detectable perturbations for any of the aromatic resonances were seen in the presence of WTpep (Fig. 9*B*). Therefore, it seems likely that Tyr^{117} does play a role in substrate recognition, although no definitive conclusion can be reached for the role of Phe^{124}. As alluded to earlier by Lescop *et al.* (34), Leu^{40} in the so-called W-loop superimposes well on the specific resi-

[5] C. Grangeasse, unpublished data.

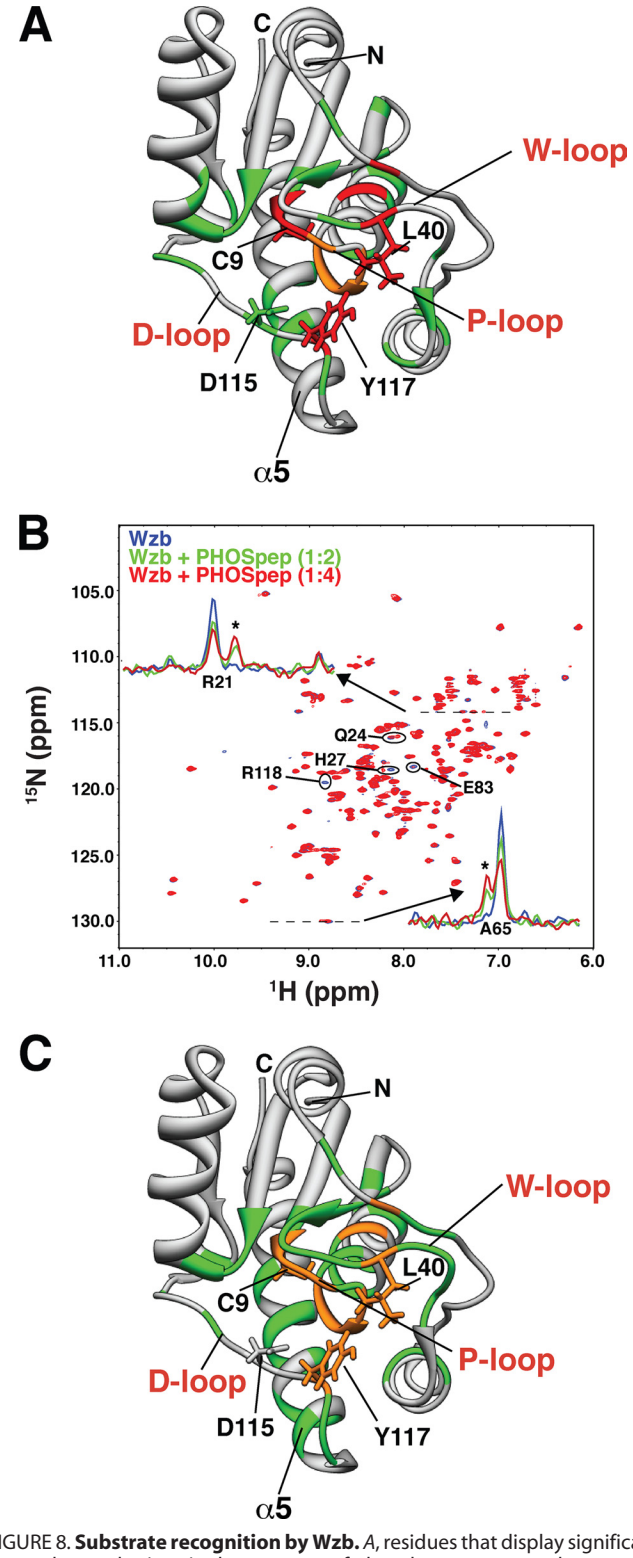

FIGURE 8. **Substrate recognition by Wzb.** *A*, residues that display significant spectral perturbations in the presence of phosphate are mapped onto a *ribbon representation* of Wzb. Residues that display chemical shift changes greater than 0.04 ppm (mean + 2 S.D.) in the presence of 5 mol eq of phosphate are *colored green*. Residues for which the corresponding amide resonances can only be seen in the presence of 200 mol eq of phosphate (Cys^{9}, Val^{10}, Glu^{20}, Leu^{40}, and Tyr^{117}) are *colored red*. Backbone amide resonances of Gly^{11}, Ile^{13}, Cys^{14}, and Arg^{15} (*colored orange*) can only be observed in phosphate buffer (50 mM phosphate, 500 mol eq). *B*, although no significant spectral perturbations in ^{15}N,^{1}H HSQC spectra of Wzb can be seen in the presence of either WTpep or MUTpep, major perturbations are seen in the presence of PHOSpep (data for 2 and 4 mol eq shown). A small subset of Wzb resonances that are attenuated in the presence of PHOSpep are *circled* and labeled. One-dimensional slices through resonances corresponding to Arg^{21} and Ala^{65} demonstrate the appearance of new peaks (indicated by the *asterisk*) in the presence of increasing concentrations of PHOSpep, indicative of slow exchange on the chemical shift time scale. *C*, spectral perturbations from *B* (for 4 mol eq of PHOSpep) are mapped onto a *ribbon representation* of Wzb. Residues for which the backbone amide resonances display attenuations of more than 0.38 (averaged over two independent measurements, greater than the mean + 3 S.D.) in the presence of the peptide are *colored green*. Residues that are not observable due to exchange broadening (Cys^{9}, Val^{10}, Gly^{11}, Ile^{13}, Cys^{14}, Arg^{15}, Glu^{20}, Leu^{40}, and Tyr^{117}) are *colored orange*. Key residues discussed in this work are labeled. Helix α5, which shows an increase in spectral perturbations (in relative terms) in the presence of PHOSpep compared with phosphate (*A*), is also labeled.

dues in eukaryotic LMW-PTPs that have been shown to play a central role in substrate recognition. Although the ^{15}N,^{1}H resonances of Leu^{40} are not visible in the absence of phosphate, the methyl positions of Leu^{40} are significantly attenuated in the presence of PHOSpep (Fig. 9*C*) but not WTpep (Fig. 9*D*). Thus, our results provide evidence supporting the conjecture (34) that the tyrosine moiety of the substrate phosphotyrosine is stabilized through ring-stacking interactions with a conserved D-loop aromatic residue, and additional stability is imparted through hydrophobic interactions with the W-loop.

In Vitro Dephosphorylation of Wzc$_{CD}$ by Wzb and Role of the EXXRXXR Motif—In order to ascertain the functional relevance of the NMR-determined binding site for Wzb on Wzc$_{CD}$, we determined the influence of mutations on the conserved E*XX*R*XX*R motif of Wzc$_{CD}$ on its ability to interact with Wzb and to be dephosphorylated by it. For this purpose, we chose a Wzc$_{CD}$ construct bearing a E508A/R511A/R514A triple mutation (Wzc$_{CD,ERR/A}$; see Fig. 3). It has been previously shown that *E. coli* cells complemented with this mutant produced 70% less colanic acid when compared with those carrying wild-type Wzc (19). As shown by the sensorgram in Fig. 10*A* (the scale is the same as in Fig. 5, *C* and *D*), Wzc$_{CD,ERR/A}$ appears to bind very weakly to Wzb. In addition, wild-type Wzc$_{CD}$ is dephosphorylated more rapidly by Wzb compared with Wzc$_{CD,ERR/A}$ (*i.e.* ~94% compared with ~69% after a 30-min incubation for a 20:1 ratio) (Fig. 10*B*). However, not surprisingly, our attempts to quantitatively analyze the dephosphorylation kinetics and obtain K_m and k_{cat} values were unsuccessful, given the multiply (and heterogeneously, as mentioned above) phosphorylated YC. A somewhat meaningful set of results could be obtained assuming the presence of two sets of sites on the YC: one set that could be dephosphorylated by Wzb in a highly efficient fashion and a second set that is dephosphorylated with lower efficiency (data not shown). This behavior is somewhat evident by the biexponential behavior displayed by the curves shown in Fig. 10*B*. To obtain more quantitative K_m and k_{cat} values, we created Wzc$_{CD}$ and Wzc$_{CD,ERR/A}$ mutants that contain a single phosphorylatable tyrosine on the C-tail. These mutants (Fig. 3), named Wzc$_{CD,F5}$ and Wzc$_{CD,ERR/A,F5}$, contain a single tyrosine (Tyr^{715}) in the YC, with all other C-tail tyrosine residues mutated to phenylalanine (Y705F, Y708F, Y710F, Y711F, and Y713F). Tyr^{715} from each Wzc$_{CD}$ subunit was found to engage the active site of a neighboring subunit in the crystal structure (19) of the Wzc$_{CD}$ oligomer. Hence, retaining Tyr^{715} was the obvious choice for the enzymatic assays. The dephosphorylation data corresponding to these mutants could be fitted to sin-

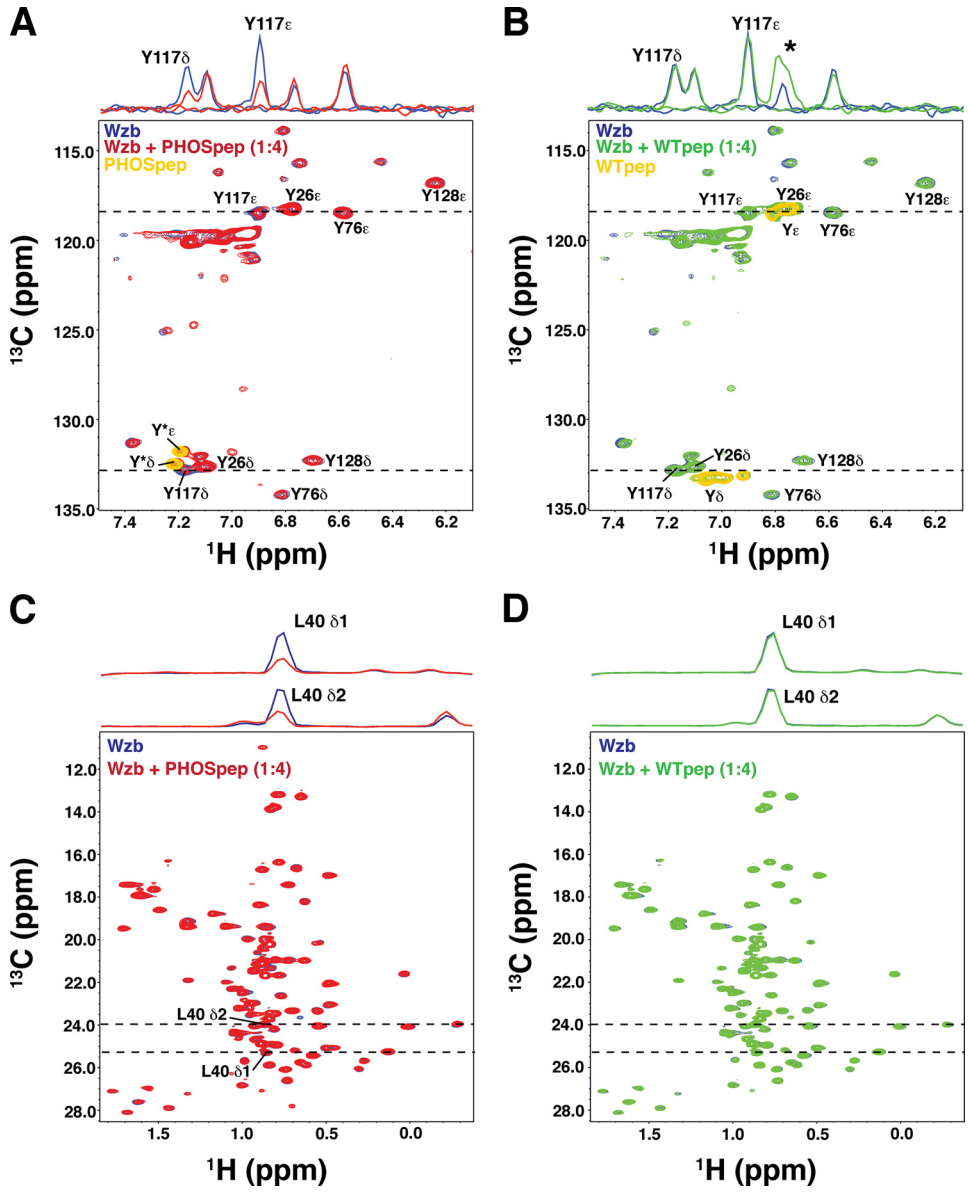

FIGURE 9. **Side chain spectral perturbations in Wzb.** ^{13}C,^{1}H HSQC spectra focusing on the aromatic (*A* and *B*) or methyl (*C* and *D*) resonances of Wzb in the presence of 4 mol eq of PHOSpep (*A* and *C*) or WTpep (*B* and *D*). One-dimensional traces (the locations of these traces in the two-dimensional spectra are indicated by the *dashed lines*; the traces for *C* and *D* are *expanded* to allow better visualization) of key perturbed resonances are shown *above* the two-dimensional spectra. In all cases, the resonances of Wzb in the apo-state are shown in *blue*, whereas those in the presence of PHOSpep or WTpep are shown in *red* and *green*, respectively. For *B*, the *asterisk* in the one-dimensional trace represents an overlap of the resonances of free WTpep with that of Y26ϵ, leading to the illusion of an increase in Wzb resonance intensity in the presence of WTpep. Resonances for the free peptides, PHOSpep (*A*) (where Y* represents the 4-phosphomonomethylphenylalanine moiety) and WTpep (*B*), are shown in *yellow* in the two-dimensional spectra.

gle-exponential functions (*e.g.* for a 35:1 kinase/phosphatase ratio, the dephosphorylation rate is 1.81 ± 0.06 min^{-1} for $Wzc_{CD,F5}$ and 0.28 ± 0.20 min^{-1} for $Wzc_{CD,ERR/A,F5}$) (Fig. 10*C*). Analysis of the enzyme kinetics in a Hanes-Woolf framework (Fig. 10*D*) confirmed that the decreased dephosphorylation rate was indeed the result of the reduced ability of $Wzc_{CD,ERR/A,F5}$ (K_m = 0.84 ± 0.28 μM) compared with $Wzc_{CD,F5}$ (K_m = 0.04 ± 0.31 μM) to form an enzyme-substrate complex with Wzb. On the other hand, the k_{cat} for $Wzc_{CD,F5}$ is only ~3.5-fold higher than that for $Wzc_{CD,ERR/A,F5}$. One may therefore conclude that mutations in the conserved E*XXR*X*XR* motif on the α2 helix of Wzc_{CD} lead to a reduction in its affinity for Wzb, resulting in a decrease in the efficiency of dephosphorylation.

In Vitro Dephosphorylation of Wzc_{CD} by Wzb and Role of the Wzb Residues Leu^{40} and Tyr^{117}—In order to test the importance of the W-loop Leu^{40} and the D-loop Tyr^{117} in the Wzb catalyzed dephosphorylation of WzcCD *in vitro*, we created Wzb mutants Wzb_{L40A}, Wzb_{Y117A}, and the double mutant $Wzb_{L40A/Y117A}$. Although the activity of Wzb_{L40A} appeared to be marginally lower than that of wild-type Wzb, Wzb_{Y117A} (and the $Wzb_{L40A/Y117A}$ double mutant) was significantly less efficient in dephosphorylating Wzc_{CD} (see Fig. 11). This suggests that although Leu^{40} may play a secondary role in interacting with the phosphotyrosine substrate, as suggested by the NMR studies described above, its involvement is less critical than that of Tyr^{117}.

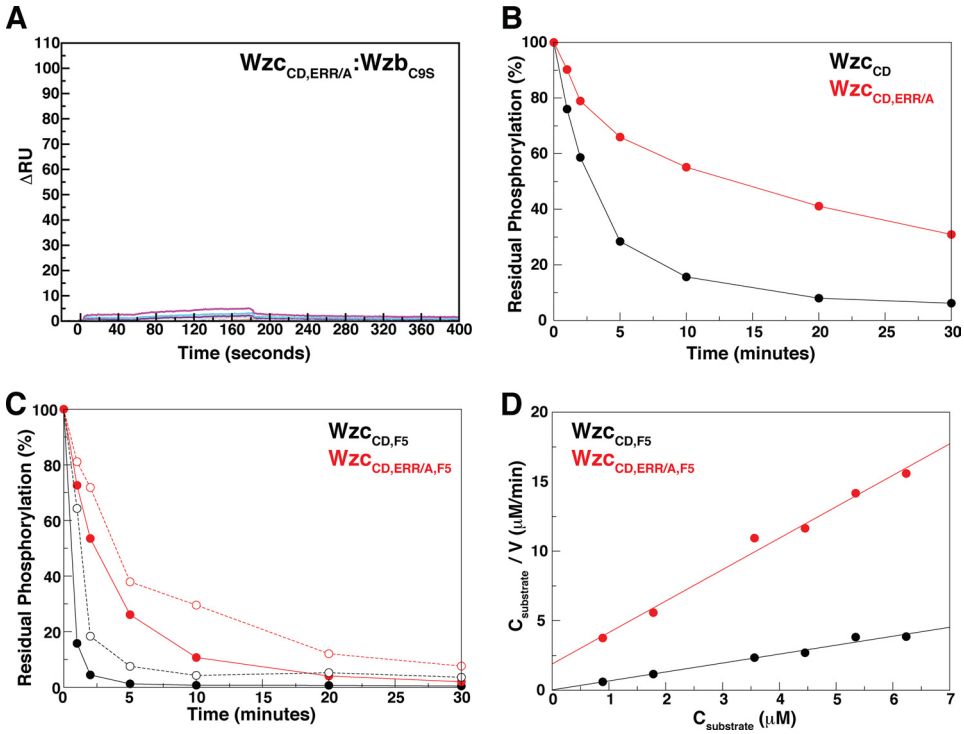

FIGURE 10. **Dephosphorylation of wild-type and mutated Wzc$_{CD}$ by Wzb.** *A*, sensorgram of the interaction of Wzc$_{CD,ERR/A}$ (ligand) with Wzb$_{C9S}$ (analyte) (the scale is the same as in Fig. 5, *C* and *D*). *B*, time course of Wzb-catalyzed dephosphorylation of Wzc$_{CD}$ (*black*) or Wzc$_{CD,ERR/A}$ (*red*). Data for a kinase/phosphatase ratio of 20:1 is shown as a representative example. *C*, time course of Wzb-catalyzed dephosphorylation of Wzc$_{CD,F5}$ (*black*) or Wzc$_{CD,ERR/A,F5}$ (*red*). Data for kinase/phosphatase ratios of 35:1 (*solid lines*) and 5:1 (*dashed lines*) are shown as representative examples. *D*, Hanes-Woolf fits using either Wzc$_{CD,F5}$ (*black*) or Wzc$_{CD,ERR/A,F5}$ (*red*) as substrates for Wzb.

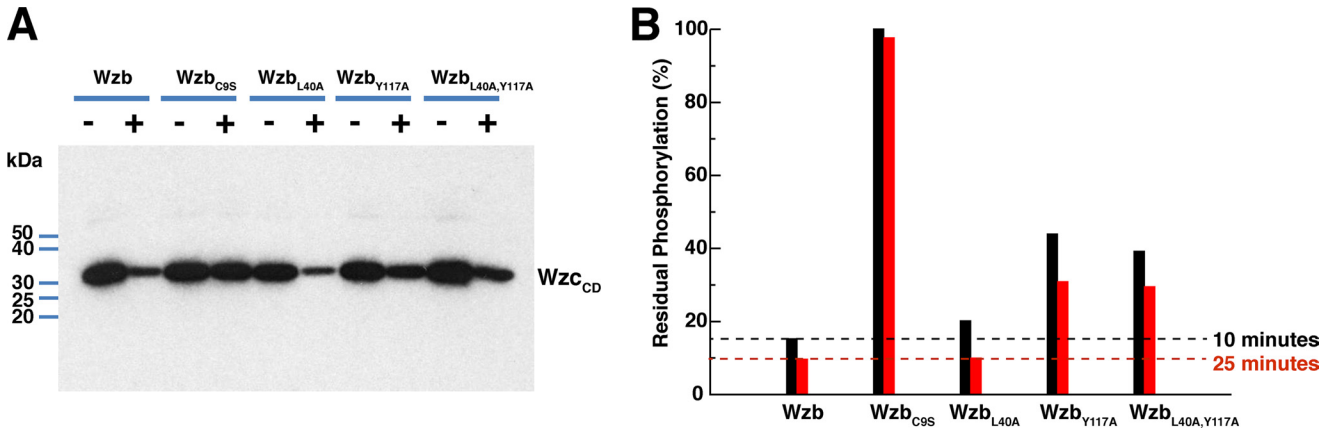

FIGURE 11. **Dephosphorylation of Wzc$_{CD}$ by wild-type and mutated Wzb.** Mutation of Tyr^{117} on the Wzb D-loop to alanine significantly reduces its ability to dephosphorylate Wzc$_{CD}$, whereas mutation of the W-loop Leu^{40} to alanine has only a minor effect. Also shown are data for the L40A/Y117A double mutant. Data for the catalytically dead Wzb mutant (Wzb$_{C9S}$) and wild-type Wzb are also shown for comparison. *A*, autoradiogram obtained after incubation of phosphorylated Wzc$_{CD}$ with Wzb and mutants thereof for a 10-min period. *B*, residual phosphorylation after 10-min (*black*) and 25-min (*red*) incubation periods. The intensities are normalized against the 10-min data for Wzb$_{C9S}$. The *dotted lines* serve as guides for the residual phosphorylation levels when using wild-type Wzb.

DISCUSSION

Maintenance of the natural equilibrium between the YC$_{high}$ and YC$_{low}$ states of Wzc, a direct result of the activity of the cytosolic LMW-PTP Wzb, appears to be critical for the production of colanic acid and survival under stress (43). Here, we have used a variety of methods to ascertain the structural elements that mediate Wzc/Wzb interactions that are central in regulating the BY-kinase signaling pathway. Using SPR measurements, we have found that a majority of the binding energy for the interactions of Wzc with Wzb is provided by elements external to the phosphorylated YC of the former. Perturbations in solution NMR spectra reveal that the Wzb binding surface on Wzc involves a region that does not include any of the Wzc catalytic elements but involves the α2 helix bearing a motif (E*XX*R*XX*R) that is highly conserved in BY-kinases, in addition to elements that are spatially proximate to it. In fact, most of the perturbations, including and around the E*XX*R*XX*R motif, involve extensive line broadening rather than chemical shift perturbations. We attribute these effects to the direct binding event that occurs on the intermediate exchange regime on the chemical shift time scale. The chemical shift perturbations, indicative of fast exchange, occur peripheral to the binding site and likely

represent conformational changes occurring upon Wzb binding. A more detailed parsing of these effects can only be achieved upon the availability of an atomic resolution model of the Wzc_{CD}-Wzb complex and a detailed analysis of the changes in dynamics upon complex formation. The critical role of the E*XX*R*XX*R motif in binding Wzb is confirmed by binding studies and biochemical assays, which reveal that mutations in this motif greatly reduce the ability of Wzc_{CD} to interact with and be dephosphorylated by Wzb. As discussed above, many lines of data indicate that the E*XX*R*XX*R motif plays a key role in the formation of asymmetric oligomers of Wzc_{CD}, allowing the YC of one molecule to access the catalytic site of another, a necessary condition to allow the intermolecular autophosphorylation. Our present results add a new wrinkle to this model, suggesting that not only does Wzb generate YC_{low} states from the YC_{high} states through its enzymatic activity, but it also probably prevents the reassociation (and consequent phosphorylation) of the Wzc_{CD} monomers. One may speculate that the purpose of this protection is to allow the active site of Wzc_{CD}, which is occluded in the oligomeric state, to be accessible to downstream targets, such as Ugd (32). The studies presented here involve the isolated CD of Wzc. It is quite possible that conformation of Wzc_{CD} and its interactions with Wzb may be modulated by periplasmic events involving the ectodomain of Wzc and indeed its trans-membrane segments. Transmission of extracytoplasmic events through the membrane to modulate the activity of cytoplasmic kinase domains has been extensively investigated in eukaryotic receptor tyrosine kinases, most notably the epidermal growth factor receptor (58, 59). In addition, cytoplasmic events, including post-translation modifications, such as phosphorylation, could also modify the interactions between Wzc_{CD} and Wzb. This mode of regulation has been seen in eukaryotic tyrosine phosphatases. For example, in T-cells, the hematopoietic PTP docks onto the mitogen-activated protein kinase (MAPK), ERK2, using a conserved D-site sequence (60). The hematopoietic PTP stays bound to ERK2 even after dephosphorylating the phosphorylated tyrosine on the activation loop of ERK2 and sequesters the inactive kinase to the cytosol (61). Detachment occurs upon phosphorylation of a D-site serine on hematopoietic PTP by protein kinase A (PKA) (62). This is an intriguing scenario, especially because it has recently been shown that Etp, the cognate LMW-PTP for Etk, is phosphorylated on a D-loop tyrosine by a yet unknown cellular kinase that is neither Etk nor Wzc (63). However, we have not yet found compelling evidence that the corresponding tyrosine (Tyr^{117}) in Wzb is phosphorylated in the cellular milieu.

As mentioned previously, the interaction of Wzb with Wzc_{CD} does not seem to require the phosphorylated YC. The use of motifs for docking interactions external to the substrate moiety to enhance affinity and specificity has been well documented in eukaryotic phosphatases (64, 65). Our results further demonstrate that the catalytic site of Wzb, especially the P-loop bearing the conserved C*XXXXX*RS motif, undergoes conformational changes upon docking interactions with $Wzc_{CD\Delta C}$ that lacks the YC. This contrasts with interactions on the Wzc_{CD} side that do not seem to display any discernable allosteric effects at its active site. Thus, docking interactions outside the Wzb catalytic site appear to trigger conformational changes in the catalytic P-loop, perhaps priming it for catalysis. Wzb undergoes significant conformational changes in the presence of phosphate, with most of these changes localized on the catalytic P-loop, on the D-loop, and, to a lesser extent, on the W-loop. Stehle *et al.* (66) have recently solved the structure of MptpA from *Mycobacterium tuberculosis* in the phosphate-free form. This structure, which represents the first LMW-PTP structure in the absence of phosphate, provides a means to compare the conformational changes expected upon phosphate binding given that the crystal structure of MptpA bound to a phosphomimetic chloride ion exists (67). In this study, Stehle *et al.* (66) show that MptpA adopts an open structure in the absence of phosphate with the D- and P-loops more distant from each other, whereas the presence of chloride induces a more closed conformation, greatly reducing the distance between the two loops. The perturbations seen in the Wzb D- and P-loops in our case are consistent with these observations. We further note the presence of extensive conformational exchange in the P-loop in the absence of phosphate, as reflected by the missing resonances. This conformational sampling is greatly reduced in the presence of phosphate, a fact that has also been previously demonstrated (34). Thus, the phosphate group of the phosphotyrosine moiety appears critical in substrate recognition by Wzb. The tyrosine moiety is stabilized largely by ring-stacking interactions with the D-loop tyrosine (Tyr^{117}) and hydrophobic interactions with a W-loop leucine (Leu^{40}). Notably, the Tyr^{117} position is strictly conserved in bacterial LMW-PTPs (Phe^{120} in *Bacillus subtilis*; see Fig. 2*A*), whereas the Leu^{40} position, although less strictly conserved, always contains a large hydrophobic residue. The central role of Tyr^{117} in stabilizing the substrate, in what is likely an optimal orientation for catalysis, is confirmed by the fact that the phosphotyrosine phosphatase activity of Wzb is significantly reduced in a Y117A mutant. Considering all of the results presented here, it seems that docking interactions between Wzc and Wzb bring the phosphorylated YC close to the catalytic site of Wzb. Dephosphorylation by Wzb proceeds due to the high local concentration of the substrate, phosphorylated YC, despite the low inherent affinity of Wzb for the isolated phospho-YC. Thus, YC dephosphorylation by Wzb may therefore be appropriately described as proximity-mediated (68).

In conclusion, we have, for the very first time, presented a comprehensive analysis of the interactions between the catalytic domain of the BY-kinase Wzc with its cognate phosphatase, Wzb. We have identified elements within the catalytic domain of Wzc that are crucial for the recognition of Wzb. In addition, our studies provide insight into the recognition by Wzb of the phosphorylated YC of Wzc, its natural substrate. These results represent a major step forward in obtaining a comprehensive understanding of the regulation of the BY-kinase signaling pathway by bacterial PTPs.

Acknowledgments—We thank Dr. Wolfgang Peti (Brown University) and Dr. David Jeruzalmi (City College of New York) for critical comments on the manuscript. We thank Dr. Zimei Bu (City College of New York) for help with the SPR measurements.

REFERENCES

1. Hunter, T. (2009) Tyrosine phosphorylation. Thirty years and counting. *Curr. Opin. Cell Biol.* **21,** 140–146
2. Manaï, M., and Cozzone, A. J. (1982) Endogenous protein phosphorylation in *Escherichia coli* extracts. *Biochem. Biophys. Res. Commun.* **107,** 981–988
3. Duclos, B., Grangeasse, C., Vaganay, E., Riberty, M., and Cozzone, A. J. (1996) Autophosphorylation of a bacterial protein at tyrosine. *J. Mol. Biol.* **259,** 891–895
4. Grangeasse, C., Doublet, P., Vaganay, E., Vincent, C., Delácuteeage, G., Duclos, B., and Cozzone, A. J. (1997) Characterization of a bacterial gene encoding an autophosphorylating protein tyrosine kinase. *Gene* **204,** 259–265
5. Byrne, J. P., Morona, J. K., Paton, J. C., and Morona, R. (2011) Identification of *Streptococcus pneumoniae* Cps2C residues that affect capsular polysaccharide polymerization, cell wall ligation, and Cps2D phosphorylation. *J. Bacteriol.* **193,** 2341–2346
6. O'Riordan, K., and Lee, J. C. (2004) *Staphylococcus aureus* capsular polysaccharides. *Clin. Microbiol. Rev.* **17,** 218–234
7. Morona, J. K., Morona, R., and Paton, J. C. (2006) Attachment of capsular polysaccharide to the cell wall of *Streptococcus pneumoniae* type 2 is required for invasive disease. *Proc. Natl. Acad. Sci. U.S.A.* **103,** 8505–8510
8. Cozzone, A. J., Grangeasse, C., Doublet, P., and Duclos, B. (2004) Protein phosphorylation on tyrosine in bacteria. *Arch. Microbiol.* **181,** 171–181
9. Grangeasse, C., Cozzone, A. J., Deutscher, J., and Mijakovic, I. (2007) Tyrosine phosphorylation. An emerging regulatory device of bacterial physiology. *Trends Biochem. Sci.* **32,** 86–94
10. Bechet, E., Guiral, S., Torres, S., Mijakovic, I., Cozzone, A. J., and Grangeasse, C. (2009) Tyrosine-kinases in bacteria. From a matter of controversy to the status of key regulatory enzymes. *Amino Acids* **37,** 499–507
11. Grangeasse, C., Nessler, S., and Mijakovic, I. (2012) Bacterial tyrosine kinases. Evolution, biological function and structural insights. *Philos. Trans. R. Soc. Lond. B Biol. Sci.* **367,** 2640–2655
12. Grangeasse, C., Terreux, R., and Nessler, S. (2010) Bacterial tyrosine-kinases. Structure-function analysis and therapeutic potential. *Biochim. Biophys. Acta* **1804,** 628–634
13. Jadeau, F., Bechet, E., Cozzone, A. J., Deléage, G., Grangeasse, C., and Combet, C. (2008) Identification of the idiosyncratic bacterial protein tyrosine kinase (BY-kinase) family signature. *Bioinformatics* **24,** 2427–2430
14. Lacour, S., Bechet, E., Cozzone, A. J., Mijakovic, I., and Grangeasse, C. (2008) Tyrosine phosphorylation of the UDP-glucose dehydrogenase of *Escherichia coli* is at the crossroads of colanic acid synthesis and polymyxin resistance. *PLoS One* **3,** e3053
15. Kolot, M., Gorovits, R., Silberstein, N., Fichtman, B., and Yagil, E. (2008) Phosphorylation of the integrase protein of coliphage HK022. *Virology* **375,** 383–390
16. Petranovic, D., Michelsen, O., Zahradka, K., Silva, C., Petranovic, M., Jensen, P. R., and Mijakovic, I. (2007) *Bacillus subtilis* strain deficient for the protein-tyrosine kinase PtkA exhibits impaired DNA replication. *Mol. Microbiol.* **63,** 1797–1805
17. Jers, C., Soufi, B., Grangeasse, C., Deutscher, J., and Mijakovic, I. (2008) Phosphoproteomics in bacteria. Towards a systemic understanding of bacterial phosphorylation networks. *Expert Rev. Proteomics* **5,** 619–627
18. Lee, D. C., Zheng, J., She, Y. M., and Jia, Z. (2008) Structure of *Escherichia coli* tyrosine kinase Etk reveals a novel activation mechanism. *EMBO J.* **27,** 1758–1766
19. Bechet, E., Gruszczyk, J., Terreux, R., Gueguen-Chaignon, V., Vigouroux, A., Obadia, B., Cozzone, A. J., Nessler, S., and Grangeasse, C. (2010) Identification of structural and molecular determinants of the tyrosine-kinase Wzc and implications in capsular polysaccharide export. *Mol. Microbiol.* **77,** 1315–1325
20. Olivares-Illana, V., Meyer, P., Bechet, E., Gueguen-Chaignon, V., Soulat, D., Lazereg-Riquier, S., Mijakovic, I., Deutscher, J., Cozzone, A. J., Laprévote, O., Morera, S., Grangeasse, C., and Nessler, S. (2008) Structural basis for the regulation mechanism of the tyrosine kinase CapB from *Staphylococcus aureus*. *PLoS Biol.* **6,** e143
21. Hanks, S. K., and Hunter, T. (1995) Protein kinases 6. The eukaryotic protein kinase superfamily. Kinase (catalytic) domain structure and classification. *FASEB J.* **9,** 576–596
22. Jadeau, F., Grangeasse, C., Shi, L., Mijakovic, I., Deléage, G., and Combet, C. (2012) BYKdb. The bacterial protein tyrosine kinase database. *Nucleic Acids Res.* **40,** D321–D324
23. Vincent, C., Duclos, B., Grangeasse, C., Vaganay, E., Riberty, M., Cozzone, A. J., and Doublet, P. (2000) Relationship between exopolysaccharide production and protein-tyrosine phosphorylation in gram-negative bacteria. *J. Mol. Biol.* **304,** 311–321
24. Cowan-Jacob, S. W. (2006) Structural biology of protein tyrosine kinases. *Cell Mol. Life Sci.* **63,** 2608–2625
25. Parsons, S. J., and Parsons, J. T. (2004) Src family kinases, key regulators of signal transduction. *Oncogene* **23,** 7906–7909
26. Boggon, T. J., and Eck, M. J. (2004) Structure and regulation of Src family kinases. *Oncogene* **23,** 7918–7927
27. Tsygankov, A. Y. (2003) Non-receptor protein tyrosine kinases. *Front. Biosci.* **8,** s595–s635
28. Paiment, A., Hocking, J., and Whitfield, C. (2002) Impact of phosphorylation of specific residues in the tyrosine autokinase, Wzc, on its activity in assembly of group 1 capsules in *Escherichia coli*. *J. Bacteriol.* **184,** 6437–6447
29. Doublet, P., Grangeasse, C., Obadia, B., Vaganay, E., and Cozzone, A. J. (2002) Structural organization of the protein-tyrosine autokinase Wzc within *Escherichia coli* cells. *J. Biol. Chem.* **277,** 37339–37348
30. Chen, H., Xu, C.-F., Ma, J., Eliseenkova, A. V., Li, W., Pollock, P. M., Pitteloud, N., Miller, W. T., Neubert, T. A., and Mohammadi, M. (2008) A crystallographic snapshot of tyrosine trans-phosphorylation in action. *Proc. Natl. Acad. Sci. U.S.A.* **105,** 19660–19665
31. Collins, R. F., Beis, K., Dong, C., Botting, C. H., McDonnell, C., Ford, R. C., Clarke, B. R., Whitfield, C., and Naismith, J. H. (2007) The 3D structure of a periplasm-spanning platform required for assembly of group 1 capsular polysaccharides in *Escherichia coli*. *Proc. Natl. Acad. Sci. U.S.A.* **104,** 2390–2395
32. Grangeasse, C., Obadia, B., Mijakovic, I., Deutscher, J., Cozzone, A. J., and Doublet, P. (2003) Autophosphorylation of the *Escherichia coli* protein kinase Wzc regulates tyrosine phosphorylation of Ugd, a UDP-glucose dehydrogenase. *J. Biol. Chem.* **278,** 39323–39329
33. Mijakovic, I., Poncet, S., Boël, G., Mazé, A., Gillet, S., Jamet, E., Decottignies, P., Grangeasse, C., Doublet, P., Le Maréchal, P., and Deutscher, J. (2003) Transmembrane modulator-dependent bacterial tyrosine kinase activates UDP-glucose dehydrogenases. *EMBO J.* **22,** 4709–4718
34. Lescop, E., Hu, Y., Xu, H., Hu, W., Chen, J., Xia, B., and Jin, C. (2006) The solution structure of *Escherichia coli* Wzb reveals a novel substrate recognition mechanism of prokaryotic low molecular weight protein-tyrosine phosphatases. *J. Biol. Chem.* **281,** 19570–19577
35. Hagelueken, G., Huang, H., Mainprize, I. L., Whitfield, C., and Naismith, J. H. (2009) Crystal structures of Wzb of *Escherichia coli* and CpsB of *Streptococcus pneumoniae*, representatives of two families of tyrosine phosphatases that regulate capsule assembly. *J. Mol. Biol.* **392,** 678–688
36. Vega, C., Chou, S., Engel, K., Harrell, M. E., Rajagopal, L., and Grundner, C. (2011) Structure and substrate recognition of the *Staphylococcus aureus* protein tyrosine phosphatase PtpA. *J. Mol. Biol.* **413,** 24–31
37. Tabernero, L., Aricescu, A. R., Jones, E. Y., and Szedlacsek, S. E. (2008) Protein tyrosine phosphatases. Structure-function relationships. *FEBS J.* **275,** 867–882
38. Vincent, C., Doublet, P., Grangeasse, C., Vaganay, E., Cozzone, A. J., and Duclos, B. (1999) Cells of *Escherichia coli* contain a protein-tyrosine kinase, Wzc, and a phosphotyrosine-protein phosphatase, Wzb. *J. Bacteriol.* **181,** 3472–3477
39. Nadler, C., Koby, S., Peleg, A., Johnson, A. C., Suddala, K. C., Sathiyamoorthy, K., Smith, B. E., Sapre, M. A., and Rosenshine, I. (2012) Cycling of Etk and Etp phosphorylation states is involved in formation of Group 4 Capsule by *Escherichia coli*. *PLoS One* **7,** e37984
40. Grangeasse, C., Doublet, P., Vincent, C., Vaganay, E., Riberty, M., Duclos, B., and Cozzone, A. J. (1998) Functional characterization of the low-molecular-mass phosphotyrosine-protein phosphatase of *Acinetobacter johnsonii*. *J. Mol. Biol.* **278,** 339–347

41. Preneta, R., Jarraud, S., Vincent, C., Doublet, P., Duclos, B., Etienne, J., and Cozzone, A. J. (2002) Isolation and characterization of a protein-tyrosine kinase and a phosphotyrosine-protein phosphatase from *Klebsiella pneumoniae*. *Comp. Biochem. Physiol. B* **131,** 103–112
42. Whitfield, C. (2006) Biosynthesis and assembly of capsular polysaccharides in *Escherichia coli*. *Annu. Rev. Biochem.* **75,** 39–68
43. Obadia, B., Lacour, S., Doublet, P., Baubichon-Cortay, H., Cozzone, A. J., and Grangeasse, C. (2007) Influence of tyrosine-kinase Wzc activity on colanic acid production in *Escherichia coli* K12 cells. *J. Mol. Biol.* **367,** 42–53
44. Mao, Y., Doyle, M. P., and Chen, J. (2006) Role of colanic acid exopolysaccharide in the survival of enterohaemorrhagic *Escherichia coli* O157:H7 in simulated gastrointestinal fluids. *Lett. Appl. Microbiol.* **42,** 642–647
45. Temel, D. B., Dutta, K., and Ghose, R. (2012) Sequence-specific ^{1}H, ^{13}C and ^{15}N assignments of the catalytic domain of the *Escherichia coli* protein tyrosine kinase, Wzc. *Biomol. NMR Assign.* DOI 10.1007/s12104-012-9448-0
46. Muratore, K. E., and Cole, P. A. (2007) A lock on phosphotyrosine signaling. *ACS Chem. Biol.* **2,** 454–456
47. Boggs, P. T., Donaldson, J. R., Byrd, R. H., and Schnabel, R. B. (1989) ODRPACK software for weighted orthogonal distance regression. *ACM Trans. Math. Software* **15,** 348–364
48. Delaglio, F., Grzesiek, S., Vuister, G. W., Zhu, G., Pfeifer, J., and Bax, A. (1995) NMRPipe. A multidimensional spectral processing system based on UNIX pipes. *J. Biomol. NMR* **6,** 277–293
49. Johnson, B. A. (2004) Using NMRView to visualize and analyze the NMR spectra of macromolecules. *Methods Mol. Biol.* **278,** 313–352
50. Salzmann, M., Pervushin, K., Wider, G., Senn, H., and Wüthrich, K. (1998) TROSY in triple-resonance experiments. New perspectives for sequential NMR assignment of large proteins. *Proc. Natl. Acad. Sci. U.S.A.* **95,** 13585–13590
51. Lemak, A., Gutmanas, A., Chitayat, S., Karra, M., Farès, C., Sunnerhagen, M., and Arrowsmith, C. H. (2011) A novel strategy for NMR resonance assignment and protein structure determination. *J. Biomol. NMR* **49,** 27–38
52. Orekhov, V. Y., and Jaravine, V. A. (2011) Analysis of non-uniformly sampled spectra with multi-dimensional decomposition. *Prog. Nucl. Magn. Reson. Spectrosc.* **59,** 271–292
53. Yamazaki, T., Forman-Kay, J., and Kay, L. E. (1993) Two-dimensional NMR experiments for correlating $^{13}C\beta$ and $^{1}H\delta/\epsilon$ chemical shifts of aromatic residues in ^{13}C-labeled proteins via scalar couplings. *J. Am. Chem. Soc.* **115,** 11054–11055
54. Zhu, G., Xia, Y., Nicholson, L. K., and Sze, K. H. (2000) Protein dynamics measurements by TROSY-based NMR experiments. *J. Magn. Reson.* **143,** 423–426
55. Anthis, N. J., Haling, J. R., Oxley, C. L., Memo, M., Wegener, K. L., Lim, C. J., Ginsberg, M. H., and Campbell, I. D. (2009) β integrin tyrosine phosphorylation is a conserved mechanism for regulating talin-induced integrin activation. *J. Biol. Chem.* **284,** 36700–36710
56. Zuiderweg, E. R. (2002) Mapping protein-protein interactions in solution by NMR spectroscopy. *Biochemistry* **41,** 1–7
57. Latham, M. P., Zimmermann, G. R., and Pardi, A. (2009) NMR chemical exchange as a probe for ligand-binding kinetics in a theophylline-binding RNA aptamer. *J. Am. Chem. Soc.* **131,** 5052–5053
58. Arkhipov, A., Shan, Y., Das, R., Endres, N. F., Eastwood, M. P., Wemmer, D. E., Kuriyan, J., and Shaw, D. E. (2013) Architecture and membrane interactions of the EGF receptor. *Cell* **152,** 557–569
59. Endres, N. F., Das, R., Smith, A. W., Arkhipov, A., Kovacs, E., Huang, Y., Pelton, J. G., Shan, Y., Shaw, D. E., Wemmer, D. E., Groves, J. T., and Kuriyan, J. (2013) Conformational coupling across the plasma membrane in activation of the EGF receptor. *Cell* **152,** 543–556
60. Bardwell, L. (2006) Mechanisms of MAPK signalling specificity. *Biochem. Soc. Trans.* **34,** 837–841
61. Pettiford, S. M., and Herbst, R. (2003) The protein tyrosine phosphatase HePTP regulates nuclear translocation of ERK2 and can modulate megakaryocytic differentiation of K562 cells. *Leukemia* **17,** 366–378
62. Saxena, M., Williams, S., Taskén, K., and Mustelin, T. (1999) Crosstalk between cAMP-dependent kinase and MAP kinase through a protein tyrosine phosphatase. *Nat. Cell Biol.* **1,** 305–311
63. Nadler, C., Koby, S., Peleg, A., Johnson, A. C., Suddala, K. C., Sathiyamoorthy, K., Smith, B. E., Saper, M. A., and Rosenshine, I. (2012) Cycling of Etk and Etp phosphorylation states is involved in formation of group 4 capsule by *Escherichia coli*. *PLoS One* **7,** e37984
64. Reményi, A., Good, M. C., and Lim, W. A. (2006) Docking interactions in protein kinase and phosphatase networks. *Curr. Opin. Struct. Biol.* **16,** 676–685
65. Virshup, D. M., and Shenolikar, S. (2009) From promiscuity to precision. Protein phosphatases get a makeover. *Mol. Cell* **33,** 537–545
66. Stehle, T., Sreeramulu, S., Löhr, F., Richter, C., Saxena, K., Jonker, H. R., and Schwalbe, H. (2012) The apo-structure of the low molecular weight protein-tyrosine phosphatase A (MptpA) from *Mycobacterium tuberculosis* allows for better target-specific drug development. *J. Biol. Chem.* **287,** 34569–34582
67. Madhurantakam, C., Rajakumara, E., Mazumdar, P. A., Saha, B., Mitra, D., Wiker, H. G., Sankaranarayanan, R., and Das, A. K. (2005) Crystal structure of low-molecular-weight protein tyrosine phosphatase from *Mycobacterium tuberculosis* at 1.9 Å resolution. *J. Bacteriol.* **187,** 2175–2181
68. Rainey, M. A., Callaway, K., Barnes, R., Wilson, B., and Dalby, K. N. (2005) Proximity-induced catalysis by the protein kinase ERK2. *J. Am. Chem. Soc.* **127,** 10494–10495